3-23-2018

The Geographic Distribution of Downburst Frequency across Spaceport Florida

Tania M. Garza

THE GEOGRAPHIC DISTRIBUTION OF DOWNBURST FREQUENCY ACROSS SPACEPORT FLORIDA

THESIS

Tania M. Garza, Captain, USAF

AFIT-ENP-MS-18-M-082

DEPARTMENT OF THE AIR FORCE
AIR UNIVERSITY

AIR FORCE INSTITUTE OF TECHNOLOGY

Wright-Patterson Air Force Base, Ohio

AFIT-ENP-MS-18-M-082

THE GEOGRAPHIC DISTRIBUTION OF DOWNBURST FREQUENCY ACROSS SPACEPORT FLORIDA

THESIS

Presented to the Faculty

Department of Engineering Physics

Graduate School of Engineering and Management

Air Force Institute of Technology

Air University

Air Education and Training Command

In Partial Fulfillment of the Requirements for the

Degree of Master of Science in Atmospheric Science

Tania M. Garza, BS

Captain, USAF

March 2018

AFIT-ENP-MS-18-M-082

THE GEOGRAPHICAL DISTRIBUTION OF DOWNBURST FREQUENCY ACROSS SPACEPORT FLORIDA

Tania M. Garza, BS

Captain, USAF

Committee Membership:

Maj O. A. Nava, PhD
Chair

William P. Roeder
Member

R. A. Stenger, PhD
Member

AFIT-ENP-MS-18-M-082

Abstract

Strong winds from downbursts pose a significant hazard to personnel and launch operations at Cape Canaveral Air Force Station (CCAFS) and NASA Kennedy Space Center (KSC). The CCAFS/KSC complex has a robust mesonet from which an 18 year (1995-2012) warm-season convective wind climatology (WSCWC) was developed (Koermer 2017). While the frequency of downbursts in the area has been determined, the frequency at the individual tower locations has not. The 5-minute peak wind data from the WSCWC was analyzed to determine the geographic distribution of downburst frequency across Spaceport Florida. For this project a downburst was determined by the peak wind threshold of greater than or equal to 35 kt. Data for each individual tower in the mesonet was analyzed with respect to the period of record, warm-season month, and flow regime. This was to determine the frequency of downburst at each grid point. A distinct pattern emerged that showed downburst maxima near the coast and minima mostly over the mainland. It appeared that the flow regimes were the driving factor for the spatial distribution of thunderstorms and subsequent downbursts (Dinon et al. 2008, McCue et al. 2010, Lupo 2013).

Acknowledgments

First, I would like to thank my advisor for his guidance and support in completing this research. He shared his personal experiences and challenges of graduate student life. This helped me cope with my own challenges. With much tact he pushed me off the fence in moments of indecision and coaxed me out of rabbit holes that I inevitably found myself in.

Next, I thank my committee members and my classmates. I would like to thank my thesis committee members for the discussions, ideas, and feedback; their support has proven to be vital in the completion of this research. A big THANK YOU to my fellow classmates, thank you for helping me get through the drudge, we will forever be siblings in misery. I especially thank the "Renaissance Man" for schooling me on the ways of ArcMap.

To my husband, I'd like to be able to thank you for your patience and support but with a preschooler running around, patience is in high demand and low supply. So, thank you for your support. I know it was tough. Thank you for sticking it out. To my daughter, thank you for making me laugh and smile.

Tania M. Garza

Table of Contents

Page

List of Figures

Page

List of Tables

THE GEOGRAPHIC DISTRIBUTION OF DOWNBURST FREQUENCY ACROSS SPACEPORT FLORIDA

I. Introduction

1.1 Background

Strong winds from convective downbursts pose a significant hazard to the people and operations of Central Florida's Space Coast. The 45th Weather Squadron (45 WS) is located at the Cape Canaveral Air Force Station (CCAFS) in Florida and is the Air Force's unit that provides weather support to America's space program at CCAFS and NASA Kennedy Space Center (Roeder et al. 2014). The Nations' space program is very sensitive to weather and has stringent weather requirements. Weather is even more important in the weeks and months leading up to launch. In this time of ground processing there are thousands of people at work utilizing equipment worth billions of dollars to prepare the rockets, payloads, and launch pads for a space launch. Convective wind warnings issued by the 45 WS for safety and resource protection are the second leading cause for scrubs and delays to space launch.

1.2 Problem Statement

Wet microbursts are a prevalent phenomenon during Florida's warm season (WS) and are the primary cause of strong convective winds that result (Sanger 1999). The frequency of downbursts for the overall area is well known; however, the frequency at individual locations is not. The forecasters at the 45 WS are responsible for issuing accurate watches, warnings, and advisories for convective winds according to the

parameters in Table 1 for the entire CCAFS/KSC complex. Their objective is to minimize adverse impacts to costly operations and ensure resource protection (McCue et al. 2010; Harms et al. 1999). The convective wind warnings are based on speed thresholds of greater than or equal (GTE) to 35 kt and 50 kt at or below 300 feet above ground level (AGL) with desired lead-times of 30 and 60 minutes, respectively (McCue et al. 2010). Convective wind warnings are issued when the distinct possibility of damaging winds from a downburst are present. The importance of this research is to improve weather support to CCAFS/KSC.

1.3 Research Objectives

The objective of this research is to calculate the convective wind event (CWE) frequency per year for each of the 36 towers across the area of study (AoS). This is accomplished using the public warm-season convective wind climatology (WSCWC) previously developed by Plymouth State University (PSU). The CWE frequency per tower was calculated for the 18-year period of record (PoR), WS months (May-September), and synoptic pattern (flow regime). The results of this study are compiled in

Table 1. CCAFS/KSC Convective Wind Warning Thresholds (Lupo 2013)

Location	Criteria	Desired Lead Time
KSC (surface-300 ft)	$\geq$ 35 kt $\geq$ 50 kt	30 min 60 min
CCAFS (surface-200 ft)	$\geq$ 35 kt $\geq$ 50 kt	30 min 60 min

tables and contour maps. The maps were generated to illustrate the geographic distribution of CWE frequency with respect to each of the previously mentioned categories. The contour maps will allow for the interpolation of frequency between grid points.

1.4 Preview

The chapters to follow offer details about this research. Chapter 2 will provide information about the types and characteristics of downdrafts; statistical values as determined by previous studies from PSU; and the WS weather influences synoptic flow and mesoscale boundaries. In Chapter 3 the methodology utilized in this project will be presented and will include the details of the meteorological tower network, the CCAFS/KSC WSCWC, and how the data was used to calculate the CWE frequency per year. Chapter 4 will offer results and analysis of the frequencies with respect to the PoR, WS months, and synoptic flow. The research will conclude in Chapter 5 with the discussion of analysis and future opportunities of study.

II. Literature Review

This chapter will provide contextual information on matters relevant to this study. First, downbursts will be described because this phenomenon is the cause of strong convective winds during Florida's warm-season months. Next, is a summary of pertinent WSCWC studies accomplished by the research team at Plymouth State University (PSU). Lastly, there will be a brief discussion about synoptic regimes and local wind circulations that drive convection for the AoS.

2.1 Downbursts

Discovered by T. Theodore Fujita, a downburst is a wind system that is produced by convective weather (Wilson and Wakimoto 2001) and is defined as a strong downdraft that originates within the lower part of the cloud and descends to the ground (Rauber et al. 2008). Furthermore, in a downburst, the heaviest rain and its evaporation occur in a small concentrated area. There are two mechanisms by which downbursts form; cooling of the ambient air due to phase change and drag force. The first process, cooling, is the more important of the two. The complete or partial evaporation of rain (or melting of ice as a secondary process of cooling) may enhance the downdraft's rate of descent. The latent energy required to change the liquid precipitation to water vapor (ice to liquid) is pulled from the ambient environment. This process cools the falling air making it denser, allowing it to sink at an increased rate that is dependent on the temperature difference between the downdraft and ambient air. The second mechanism, drag force (precipitation drag), contributes to the downdrafts of all showers and thunderstorms. Each raindrop

falls under the influence of gravity, and as this occurs the drop pushes the air ahead of it. As a collective, the drag of millions of raindrops accelerates the air downward.

The downburst structure (Fig. 1, left) is characterized by a vortex ring that propagates outward from the downburst as it meets the surface (Fujita 1985). A particularly strong area of wind within the vortex is located near its base, typically within 100 to 160 feet AGL. There may be multiple rings as the result of several pulses of strong downward motion and outflows. As the rings propagate outward, they stretch and may break apart resulting in a runaway vortex roll (Fig. 1, right). First referred to as a Rotor Microburst by Fujita (1985) these rolls can cause damage equivalent to ”weak” tornadoes. A primary feature of the downburst is extreme divergence. Downbursts induce a highly sheared environment because of the straight-line flow from the center and subsequent curled winds that result in a vortex ring with a horizontal axis (Rauber et al. 2008). These strong winds and shear are most notably a hazard to aviation, and pose a significant threat to the ground processing of rockets, payloads, and the launch pad.

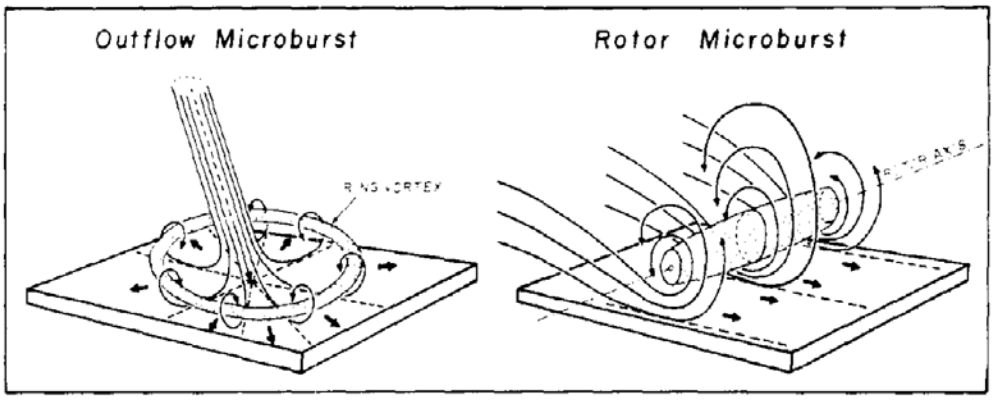

Figure 1. Microburst and subsequent rotor microburst. The ring vortex stretches with propagation away from the center point. Extreme divergence may be noted at the surface by the bolded black arrows on the left image (Fujita 1985)

2.1.1 Macroburst vs Microburst

Fujita (1985) further categorized downbursts into macroburst and microburst by the scale of damage left by the phenomena. The macroburst is defined by a pattern of damage that is > 4 km, winds as high as 116 kt, and persists for approximately 5 to 30 minutes (Sanger 1999). Smaller and more intense downbursts are defined as microbursts that have a scale of $\leq$ 4 km, winds up to 146 kt, and a life-cycle less than 10 minutes (Sanger 1999; Fujita 1985). Microbursts are subdivided into wet and dry microbursts based on statistics drawn from Northern Illinois Meteorological Research on Downbursts (NIMROD) that was conducted to determine the three-dimensional airflow structure of a downburst (Fujita 1985; Wilson and Wakimoto 2001).

2.1.2 Dry and Wet Microburst

Microbursts do not always originate from thunderstorms and may be generated from innocuous looking convective clouds (Fujita 1985). More common in the western United States and the Great Plains, dry microbursts are defined by no measurable precipitation (Rauber et al. 2008). The environment conducive for dry microbursts consists of a nearly saturated layer near 500 mb that decreases downward toward the surface, resulting in a relatively dry sub-cloud layer (Atkins and Wakimoto 1991). The winds from the dry downburst result from negative buoyancy generated by evaporation, melting, and sublimation of precipitation (Atkins and Wakimoto 1991).

In contrast to the dry microburst, the wet microburst defined by Atkins and Wakimoto (1991) is characterized by heavy precipitation observed between the onset and end of high winds. Additionally, the layer where evaporation enhances the downburst is aloft, rather than below the cloud. Wet microbursts are more common in the humid

environments of the Southern, Midwestern, and Eastern United States and are commonly observed over Florida's Space Coast (Rauber et al. 2008; Wilson and Wakimoto 2001).

Wet downbursts are the cause of convective winds during Florida's warm season (Sanger 1999). These convective winds are the second leading weather hazard behind lighting at CCAFS/KSC. For this reason, Sanger (1999) focused his study on wet microbursts and lightning across Spaceport Florida. To this end, Sanger (1999) developed a microburst climatology of warning level events based on data for the warm-season months of May to September for the years of 1995-1998. The examination of the microburst characteristics of frequency, diurnal variation, spatial variation, speed frequency distribution, and the wind direction was accomplished.

2.2 Warm-Season Convective Wind Climatology

The research team at PSU have focused effort on updating and refining the WSCWC for CCAFS/KSC. Cummings et al. (2007) looked at the data in terms of convective periods rather than by warning level microburst events. A convective period (CP) is defined as a period of convective activity that is marked by at least a 6-hour break in convection before and after the period. This definition was independent of observed wind speeds and the duration of a period varied based on the 6-hour break in convection that marked the start and end time. The climatology was updated to include all CPs, warning and non-warning levels, for 1995-2005 in order to determine if the occurrence of CPs were associated to flow regimes. The most current warm-season convective wind climatology for the 30 km x 40 km area around CCAFS/KSC now consists of 18 years of

wind observations from the CCAFS/KSC mesonet, which includes data from 82 anemometers at and below 300 ft AGL and spread across 36 weather towers.

2.3 Climate and Synoptic Flow Regimes

The humid subtropical climate of Florida's Space Coast is complicated by the natural land and water distribution (Fig. 2; McCue et al. 2010). The local weather is driven by the interaction of mesoscale boundaries that develop as a result of the weak synoptic flow and temperature difference from complex geography (McCue et al. 2010; Lupo 2013). From May to September Florida's climate is dominated by a subtropical high. The position of the ridge axis determines the prevailing low-level wind direction (Lericos et al. 2002). Lericos et al. (2002) defined eight synoptic flow regimes (Table 2). The name of the regime describes the resultant prevailing wind direction from Central to Southern Florida.

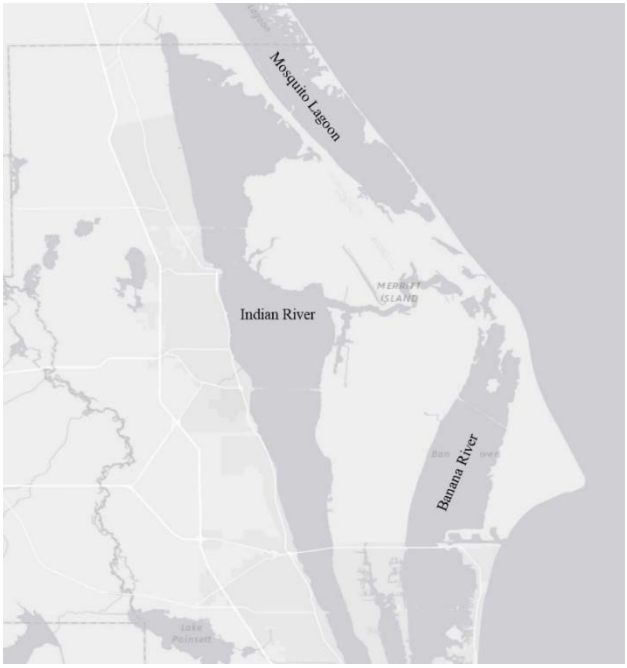

Figure 2. N**atural land-water distribution of the CCAFS/KSC complex.**

Table 2. Flow Regimes established by Lericos et al. (2002)

Flow Regime	Subtropical Ridge Position
SW-1	Subtropical ridge south of Miami
SW-2	Subtropical ridge between Miami and Tampa
NW	Subtropical ridge far to south and extending far into Gulf of Mexico and stronger
SE-1	Subtropical ridge between Tampa and Jacksonville
SE-2	Subtropical ridge north of Jacksonville
NE	Subtropical ridge far to north and extending into SE US and much stronger than normal
Other	Subtropical ridge position not defined
Missing	Missing synoptic data to determine flow regime

Lericos et al. (2002) established the warm-season synoptic patterns for the Florida Peninsula and studied how they influenced lightning activity. The regimes were based on the prevailing low level (100-700 mb) wind direction from three 12 UTC radiosonde soundings located across Florida; those stations were Jacksonville (KJAX), Tampa (KTBW), Miami (KMFL; Fig. 3). Charts illustrating the specific flow regimes may be seen in Figure 4. Lambert (2007) refined the technique to include the Cape Canaveral Air Force Station 10 UTC sounding (KXMR) when a regime was ill-defined by the previously listed soundings. This reduced the large number of "Other" and "Missing" classifications that resulted in the previous study.

Lupo (2013) examined the frequency of occurrence of all synoptic scale flow regimes for convective days for all years and found that westerly (easterly) flow regimes were most (least) commonly associated with convective activity. Cummings et al. (2007)

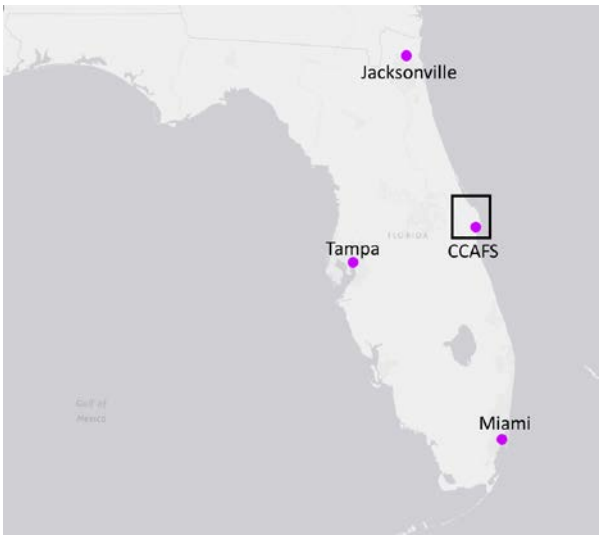

Figure 3. Radiosonde sounding locations utilized to discriminate between flow regimes (Lericos et al. 2002; Lambert 2007).

examined the distribution of warning and non-warning level winds with respect to the overall flow regime and found that westerly component flows had greater association with warning level winds compared to the regime patterns easterly component.

Convective initiation results from synoptic flow interaction with local wind circulations (Gentry and Moore 1954) such as the east and west coast sea-breeze fronts, Indian River and Banana River breeze fronts, lake breeze fronts, thunderstorm outflow boundaries, and the interaction between these and other boundaries (McCue et al. 2010). Lupo (2013) further analyzed the dataset and determined that a majority (54%) of convective events that led to warning level winds were initiated by mesoscale boundaries (SBF, OFB, and SBF & OFB). In addition, the majority of non-warning level convective winds resulted from air mass thunderstorms.

The next chapter will present the methodology of calculating the downburst frequency and mapping these values. The bootstrap statistical technique used to analyze differences in the datasets will also be described.

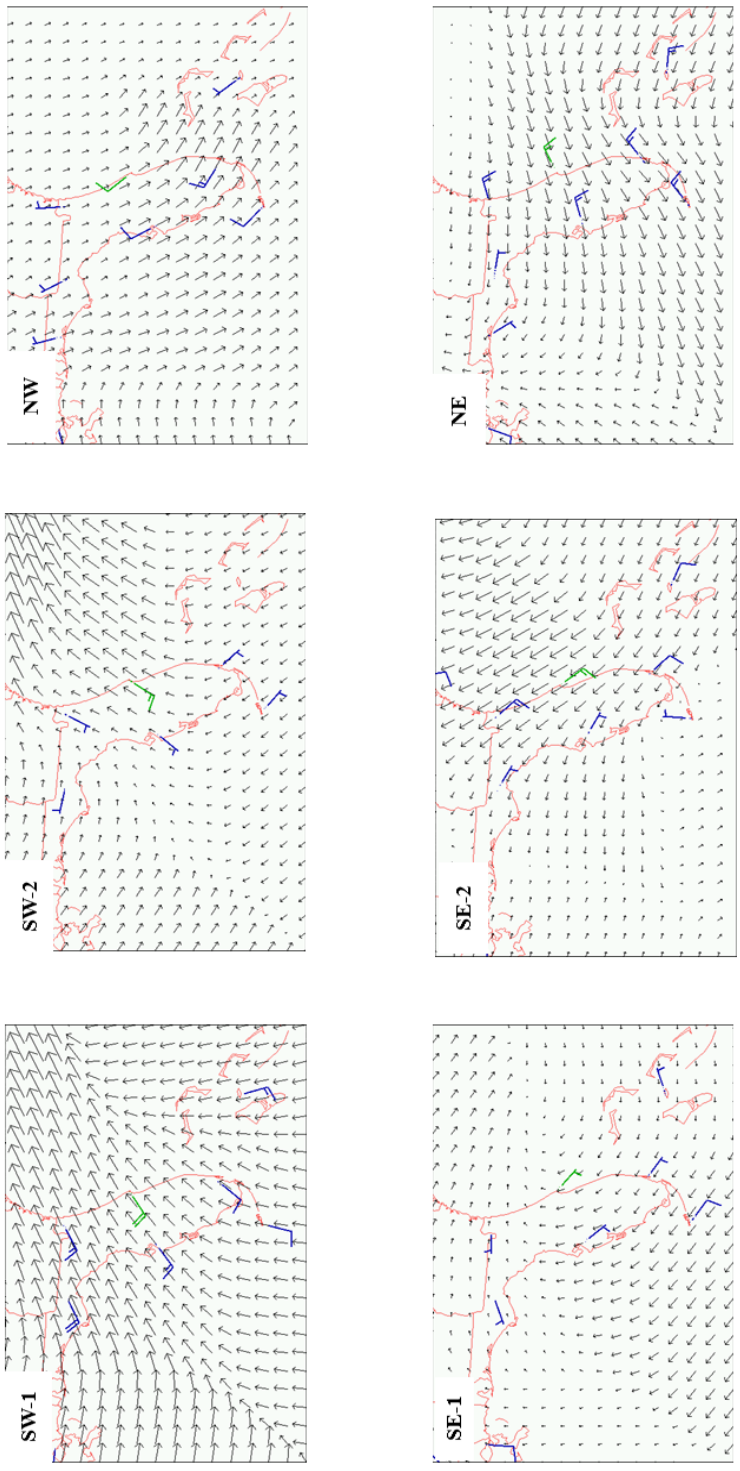

Figure 4. Mean low-level (1000-700 mb) wind vectors to depict prevailing synoptic flow per regime (Koermer 2017).

III. Methodology

This chapter will describe the methodology used to accomplish this study. The first section will describe the network of towers that observe and report peak winds. The following section will describe the WSCWC from which data was pulled to determine and map CWE frequencies for the towers across the AoS. The final section will describe the bootstrap statistical technique that will assist in the process of analysis and discussion

3.1 Mesonet

The Cape Weather Information Network Display System (Cape WINDS; ERIH handbook 2017) was and still is one of the most densely instrumented mesonets in operational meteorology (Roeder et al. 2014). The primary function of the mesonet was to collect, process, archive, and disseminate data from 36 meteorological towers across the area of study (AoS; ERIH handbook 2017). The towers were located in and around CCAFS/KSC, an area of approximately 958 km^2 (Fig. 5). The TIDs are shown in Table 3. There were six towers equipped with two sensor suites on opposite sides of the towers resulting in 42 tower identification (TID) numbers for the 36 towers. The color-filled rows in the table mark the towers with dual sensor suites; the matching colors indicate a shared tower. The table also shows the elevation of each sensor within a suite (Koermer 2017). The TID was made up of four digits, generally, the first two digits represented the tower's distance west from the coast and the last two signified the distance north of Port Canaveral; the distance is in nautical miles. Each sensor suite housed one to five anemometers of varied elevations that ranged from 12 to 492 ft above ground level

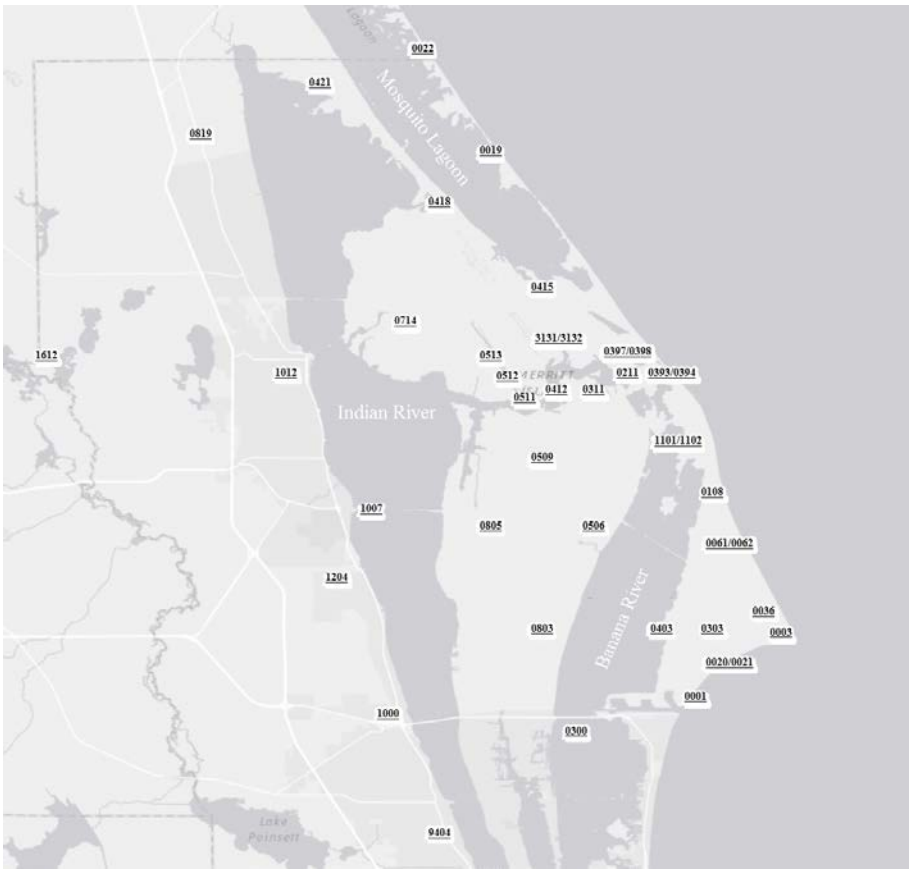

Figure 5. Depiction of tower location across the area of study.

(AGL). The sensors reported peak winds at a rate of one or five minutes. Peak winds were defined as the highest instantaneous wind speed within the time interval.

3.2 Data

The focus of this project was to analyze the data with respect to geographic location of the towers within the mesonet. The data used for this was taken from the PSU website *CCAFS/KSC Warm-Season Convective Wind Climatology* found at https://vortex.plymouth.edu/conv_winds/. It was public and available in a variety of formats. This climatology captured a range of information about convective periods (CP)

Table 3. Tower identification numbers and sensor elevations (Koermer 2017). The color-filled rows in the table mark the towers with dual sensor suites; the matching colors indicate a shared tower.

	Sensor Elevation Feet Above Ground Level (AGL)										
TID	12	30	54	60	90	145	162	204	295	394	492
0001	x		x								
0003	x		x								
0019			x								
0020	x		x		x	x		x			
0021	x		x		x	x		x			
0022			x								
0036					x						
0061	x		x				x	x			
0062	x		x				x	x			
0108	x		x								
0211	x		x								
0300			x								
0303	x		x								
0311	x		x								
0393				x							
0394				x							
0397				x							
0398				x							
0403	x		x								
0412	x		x								
0415	x		x								
0418			x								
0421			x								
0506	x		x								
0509	x		x								
0511		x									
0512		x									
0513		x									
0714	x		x								
0803	x		x								
0805	x		x								
0819			x								
1000			x								
1007			x								
1012			x								
1101	x		x				x	x			
1102	x		x				x	x			
1204			x								
1612			x								
3131	x		x				x	x	x	x	x
3132	x		x				x	x	x	x	x
9404			x								

that occurred during Florida's warm season (WS) for a span of 18 years (1995-2012; Koermer 2017). The WS on average occurred from May to September. The CP metadata included details such as 5-minute peak wind reports, KXMR soundings, radar data from Melbourne, Florida, and statistical summaries to aid in mission planning, forecast training, and operational decision-making.

The number of TIDs and sensors analyzed was slightly varied in the series of works based on the WSCWC (W. P. Roeder, personal communication, December 1, 2017). This was the result of various circumstances such as the elimination of far inland towers (Koermer and Roeder 2008) and the inclusion or exclusion of surface wind observations as towers (W. P. Roeder, personal communication, December 12, 2017). Another reason for the variance in the number of TIDs was that some works excluded data from towers that reported less than 70% of the time (Cummings et al. 2007). The PSU WSCWC omitted these towers from the database. Additionally, data from sensors above 300 ft AGL (Table 3) were omitted from the WSCWC for the purpose of supporting 45 WS's convective wind warning requirements. The WSCWC was updated and refined many times from its initial development in 1999. The data went through both an automated and a manual quality control (QC). A detailed description of the automated QC process is described by Lambert (2002). Dinon et al. (2008) and Ander et al. (2009) utilized data from the Melbourne and Tampa high resolution radars to manually refine the climatology.

3.3 Convective Wind Event

The motivation for this research was determine the CWE frequencies for each of the 42 TIDs (from this point forward TID and tower are used interchangeably) across the area and to map this data so that CWE frequency may be interpolated between towers. This was accomplished by simply dividing the total number of CWEs per tower by the number of years the tower reported peak winds with respect to three categories. These frequencies were determined for the period of record (PoR; May-September for 1995-2012); for each of the five WS months (e.g., May 1995-2012and June 1995-2012); and for the six flow regimes as described in the background section. The first step was to define CWEs, the phenomena that was being measured. The following steps were accomplished with respect to the three previously named categories. In the second step, the CWEs were compiled into a database. The third step was to examine each CWE and mark the towers that observed winds GTE 35 kt. The fourth step, was to complete a count of years a tower reported peak winds. Next, the CWE frequencies were calculated. The final step was to generate maps for the geographic distribution of CWEs frequencies with respect to the categorical datasets.

First, a CWE was defined based on the Cummings et al. (2007) definition of a CP; that was a period of convective activity that was flanked with at least a 6-hour break of no convection before and after. In other previous studies the terms CP, convective event, and convective wind event (CWE) were used interchangeably. Except in McCue et al. (2010) which defined a CWE as an event that produces a convectively generated wind gust of any speed that is recorded by one or more of the towers in the mesonet. For this project a CWE was defined as a CP for which warning level winds were observed by any

sensor at or below 300 ft AGL within the mesonet. That is to include any wind speed GTE 50 kt because the focus of this study was to determine how often warning level winds occurred at each tower without distinguishing between the GTE 35 kt and 50 kt warning levels.

The second step was to compile a database of CWEs. To best fit the requirements of this project a list was generated of all CPs from individual files posted in the WSCWC. These files were packaged as monthly data per year; a sample of the format was shown in Figure 6. This CP data summary included many items to include a list of all CP for the given month/year, the start and end time of each CP, the prevailing flow regime, and the max peak wind reported with the observation time and tower. The monthly CPs were compiled into a database with the following retained information (as shown in the first nine columns of Table 4): start and end time, month, year, and prevailing flow regime. This resulted in a list of 1149 CPs.

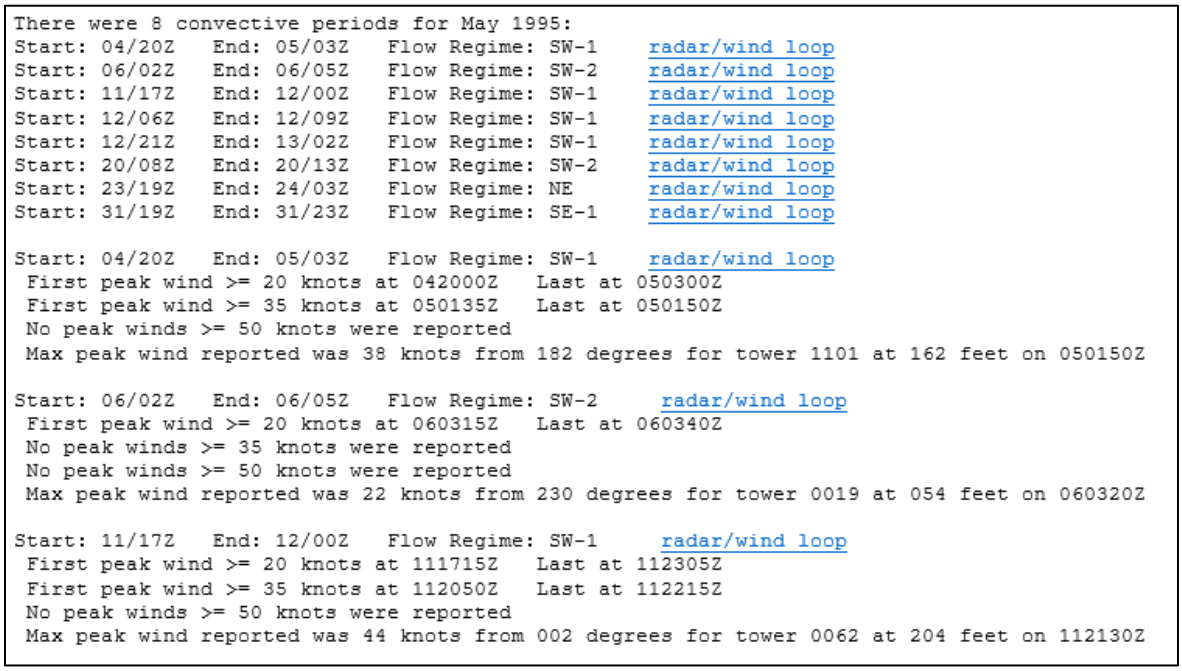

```
There were 8 convective periods for May 1995:
Start: 04/20Z   End: 05/03Z   Flow Regime: SW-1    radar/wind loop
Start: 06/02Z   End: 06/05Z   Flow Regime: SW-2    radar/wind loop
Start: 11/17Z   End: 12/00Z   Flow Regime: SW-1    radar/wind loop
Start: 12/06Z   End: 12/09Z   Flow Regime: SW-1    radar/wind loop
Start: 12/21Z   End: 13/02Z   Flow Regime: SW-1    radar/wind loop
Start: 20/08Z   End: 20/13Z   Flow Regime: SW-2    radar/wind loop
Start: 23/19Z   End: 24/03Z   Flow Regime: NE      radar/wind loop
Start: 31/19Z   End: 31/23Z   Flow Regime: SE-1    radar/wind loop

Start: 04/20Z   End: 05/03Z   Flow Regime: SW-1    radar/wind loop
 First peak wind >= 20 knots at 042000Z   Last at 050300Z
 First peak wind >= 35 knots at 050135Z   Last at 050150Z
 No peak winds >= 50 knots were reported
 Max peak wind reported was 38 knots from 182 degrees for tower 1101 at 162 feet on 050150Z

Start: 06/02Z   End: 06/05Z   Flow Regime: SW-2     radar/wind loop
 First peak wind >= 20 knots at 060315Z   Last at 060340Z
 No peak winds >= 35 knots were reported
 No peak winds >= 50 knots were reported
 Max peak wind reported was 22 knots from 230 degrees for tower 0019 at 054 feet on 060320Z

Start: 11/17Z   End: 12/00Z   Flow Regime: SW-1     radar/wind loop
 First peak wind >= 20 knots at 111715Z   Last at 112305Z
 First peak wind >= 35 knots at 112050Z   Last at 112215Z
 No peak winds >= 50 knots were reported
 Max peak wind reported was 44 knots from 002 degrees for tower 0062 at 204 feet on 112130Z
```

Figure 6. Sample of convective period summaries available in the WSCWC.

Table 4. Example of refined database.

Start	Day	UTC	End	DD	UTC	Flow	Month	Year	0001	0003	0019	0020		9404
Start	04	20	End	05	03	SW-1	May	1995	0	0	0	0		0
Start	11	17	End	12	00	SW-1	May	1995	0	0	1	0		0
Start	20	08	End	20	13	SW-2	May	1995	0	0	0	0		0
Start	23	19	End	24	03	NE	May	1995	0	0	0	0		0
Start	28	17	End	28	23	SW-2	May	1996	0	0	0	0		0
Start	30	22	End	31	7	NW	May	1996	0	1	0	1		0
Start	31	15	End	31	23	NE	May	1996	0	1	0	1		0
Start	3	16	End	4	5	SW-2	May	1997	0	0	0	1		0
Start	27	23	End	28	4	NW	May	1997	0	0	0	0		0
Start	28	15	End	28	22	NW	May	1997	0	1	0	0		0
Some CWEs intentionally left out of sample table														
Start	17	16	End	18	3	SW-2	May	2012	0	0	0	0		0
Total CWE per Tower									3	7	5	10		2
Average Years a Tower Reported Peak Winds									18	17	17	17		17
CWE Frequency per Year									0.17	0.41	0.29	0.59		0.12

Some columns intentionally left out of sample table

The list was reviewed and 1135 CPs were retained for use in this research. Table 5 was provided to show the number of CPs considered for this project. CPs were categorized in the table as CP and CP(0). The last column of CP(0) shows the number of CPs omitted from the dataset of which there were 14. The omissions resulted from one of two reasons. The first was that the wind data for an entire CP was missing. This was the case for two CPs that both occurred in 1995. The second reason was that the duration of the CP overlapped two months. Keeping these 12 CPs would have unnecessarily complicated the calculations for monthly analysis; only four of those were CWE. Omitting these CPs was insignificant to the final results because of the large sample size. A sample of the refined database for this research was shown in Table 4. It was noted that by definition all CWEs were CP but not all CP resulted in a CWE. The max peak

Table 5. Annual Count: CWEs, CP, and omitted CPs.

Year	CWE	CP	CP(0)
1995	15	47	2
1996	26	34	0
1997	24	48	2
1998	22	44	1
1999	14	48	2
2000	24	37	0
2001	30	40	0
2002	20	60	1
2003	21	44	0
2004	34	37	2
2005	25	28	0
2006	14	19	1
2007	25	30	0
2008	26	24	0
2009	39	46	1
2010	19	47	0
2011	28	37	1
2012	34	25	1
Totals	440	695	14
Total CP Retained	1135		
Total CP in WSCWC	1149		

wind information for each CP as shown in Figure 6 was reviewed. From this each of the 1135 CPs were characterized in a binary manner as having observed a 5-minute peak wind of less than 35 kt or GTE 35 kt. This resulted in the identification of 440 CWEs.

The third step was to examine five-minute peak wind observations for the period of each CWE and mark the towers that observed winds GTE 35 kt. A binary method was again utilized to specify if a tower had observed warning level winds. The WSCWC allowed for a query of 5-minute peak wind observations for all sensors; a sample is

shown in Figure 7. This information was filtered to show peak wind observations of GTE 35 kt for any sensor. From this, each tower was characterized as having observed the CWE or not. The tower was marked as having observed the strong winds if at least one sensor in the tower's suite reported a peak wind of GTE 35 kt. This resulted in a database that best fit the requirements for this project; a sample of the database is shown Table 4.

The fourth step, was to complete a count of years a tower reported peak winds. The number of years was required as the divisor to calculate CWE frequency per year for each tower. It was found that the number of years the sensors within a tower's suite reported winds was different from year to year. The number of years that sensors reported peak winds varied from 10 to 18 years. The summary, *CCAFS/KSC Peak Wind Monthly Statistical Summaries for 1995-2012 for all Convective Periods* for the category

Here are the data for all tower id's at all sensor elevations on 05/01/1995 for 0000Z-2355Z:

T_ID	Year	Mo	Day	Hr	Min	Elev	Temp(F)	TD(F)	WS(kt)	WDIR	PK(kt)	PKDIR	DDEV	RH(%)
1	1995	5	1	0	0	12	-9999.0	-9999.0	1	112	4	115	27	-9999
1	1995	5	1	0	5	12	-9999.0	-9999.0	2	104	4	88	27	-9999
1	1995	5	1	0	10	12	-9999.0	-9999.0	1	105	3	103	27	-9999
1	1995	5	1	0	15	12	-9999.0	-9999.0	2	103	5	101	25	-9999
1	1995	5	1	0	20	12	-9999.0	-9999.0	1	107	4	97	25	-9999
1	1995	5	1	0	25	12	-9999.0	-9999.0	1	116	2	95	28	-9999
1	1995	5	1	0	30	12	-9999.0	-9999.0	1	119	3	104	27	-9999
1	1995	5	1	0	35	12	-9999.0	-9999.0	0	114	3	94	31	-9999
1	1995	5	1	0	40	12	-9999.0	-9999.0	1	116	3	134	32	-9999
1	1995	5	1	0	45	12	-9999.0	-9999.0	0	115	1	150	36	-9999
1	1995	5	1	0	50	12	-9999.0	-9999.0	1	128	3	115	38	-9999
1	1995	5	1	0	55	12	-9999.0	-9999.0	1	123	3	126	38	-9999
1	1995	5	1	1	0	12	-9999.0	-9999.0	0	148	2	174	41	-9999
1	1995	5	1	1	5	12	-9999.0	-9999.0	1	126	3	107	40	-9999
1	1995	5	1	1	10	12	-9999.0	-9999.0	1	138	4	174	40	-9999
1	1995	5	1	1	15	12	-9999.0	-9999.0	1	147	5	158	40	-9999
1	1995	5	1	1	20	12	-9999.0	-9999.0	1	144	3	81	40	-9999
1	1995	5	1	1	25	12	-9999.0	-9999.0	1	141	3	114	42	-9999
1	1995	5	1	1	30	12	-9999.0	-9999.0	1	135	3	139	40	-9999
1	1995	5	1	1	35	12	-9999.0	-9999.0	1	152	4	173	40	-9999
1	1995	5	1	1	40	12	-9999.0	-9999.0	1	139	3	158	43	-9999
1	1995	5	1	1	45	12	-9999.0	-9999.0	1	144	5	150	43	-9999
1	1995	5	1	1	50	12	-9999.0	-9999.0	0	142	3	107	44	-9999
1	1995	5	1	1	55	12	-9999.0	-9999.0	1	143	3	123	43	-9999
1	1995	5	1	2	0	12	-9999.0	-9999.0	1	134	3	160	44	-9999

Figure 7. Sample of 5-minute peak wind observations from all sensors for a prescribed date (Koermer 2017).

of tower versus speed, was packaged per month of all years (e.g., May 1995-2012 and June 1995-2012); a sample is shown in Table 6. It was comprised of the count for 5-minute peak winds observations per speed categories for each sensor. The last column of this data, ALL OBS, was the focus for determining if a sensor had reported 5-minute peak winds for a given year.

A year was omitted from the count if the number of peak wind observations in the ALL OBS column was zero as seen in Table 6. The mean wind speed for KXMR in the WS months as reported in the Operational Climatic Data Summary (OCDS-II) varied from 5.4 to 6.8 kt (14 WS 2017). The OCDS-II is a climate summary package that provides multiple weather parameters and is produced by the 14th Weather Squadron. The relatively light wind speeds validated the basis for elimination of a year from the count because it was meteorologically unsound that there were zero peak wind reports for the duration of a year. In some cases, there were multiple sensors per tower for the 18-year period that had to be considered; 20 towers had one sensor and 22 towers had two or more sensors (Table 3). There were occurrences of inconsistent peak wind reports among the sensors of a suite. Therefore, the average year per tower was determined. For example, tower 0020 had five sensors at varied elevations under 300 ft AGL. For the PoR that tower had an average of 17.08 years for which it reported data because of the variation in sensor reporting. The average years a tower reported peak winds was determined for the WS months and for the PoR. These values may be seen in Table 7.

Next, the CWE frequencies per year were calculated for each tower with respect to the PoR, WS months, and synoptic pattern (as shown in the last row of the example

Table 6. Snapshot of *CCAFS/KSC Peak Wind Monthly Statistical Summaries for 1995-2012 for All CP* for the Category of Tower versus Speed (Koermer 2017)

All Periods Tower Summary May_1995															
TWR	ELEV	0- 4	5-9	10-14	15-19	20-24	25-29	30-34	35-39	40-44		85-89	90-94	95-99	ALL OBS
1	12	49	235	176	30	1	3	0	0	0		0	0	0	494
1	54	7	102	161	167	60	5	6	0	0		0	0	0	508
3	12	12	92	191	169	37	9	1	0	0		0	0	0	511
3	54	6	65	169	163	93	8	5	0	0		0	0	0	509
19	54	2	51	86	90	37	11	4	2	0		0	0	0	283
20	12	0	0	0	0	0	0	0	0	0		0	0	0	0
20	54	0	0	0	0	0	0	0	0	0		0	0	0	0
20	90	0	0	0	0	0	0	0	0	0		0	0	0	0
20	145	0	0	0	0	0	0	0	0	0		0	0	0	0
20	204	0	0	0	0	0	0	0	0	0		0	0	0	0
21	12	0	0	0	0	0	0	0	0	0	Column intentionally left blank	0	0	0	0
21	54	0	0	0	0	0	0	0	0	0		0	0	0	0
21	90	0	0	0	0	0	0	0	0	0		0	0	0	0
21	145	0	0	0	0	0	0	0	0	0		0	0	0	0
21	204	0	0	0	0	0	0	0	0	0		0	0	0	0
22	54	8	59	105	144	115	22	6	0	0		0	0	0	459
36	90	4	76	155	167	87	13	1	0	0		0	0	0	503
61	12	76	194	185	15	2	0	0	0	0		0	0	0	472
61	54	15	121	164	143	35	6	0	0	0		0	0	0	484
61	162	6	56	159	118	120	25	3	1	1		0	0	0	489
61	204	6	42	158	128	119	26	8	2	1		0	0	0	490
62	12	79	194	179	16	2	0	0	0	0		0	0	0	470
62	54	15	109	176	148	28	7	0	0	0		0	0	0	483

dataset; Table 4). To do this the data was summed per tower column (as seen near the bottom of Table 4) and then divided by the appropriate average number of years a tower reported peak winds (see Table 7). The CWE totals per tower were divided by the average years as shown in Table 7. The CWE totals for the flow regimes for each tower were divided by the average years for PoR (see Table 7). The PoR average years was

Table 7. Average years a tower reported peak winds.

Tower	May	June	July	August	September	PoR
0001	18	18	18	18	17	17.8
0003	17	17	17	17	17	17
0019	17	17	16	17	16	16.6
0020	17	17	17	17	17.4	17.08
0021	17	17	17	17	18	17.2
0022	18	18	18	18	15	17.4
0036	10	10	10	10	10	10
0061	18	18	18	18	18	18
0062	18	18	18	18	18	18
0108	17	18	18	18	18	17.8
0211	18	18	18	18	18	18
0300	18	18	18	18	18	18
0303	18	18	18	18	18	18
0311	18	18	18	18	18	18
0393	17	17	17	17	16	16.8
0394	17	17	16	16	16	16.4
0397	15	15	15	15	14	14.8
0398	15	15	15	15	13	14.6
0403	18	18	18	18	18	18
0412	18	18	18	18	18	18
0415	18	18	18	18	18	18
0418	18	18	18	18	18	18
0421	18	18	18	18	18	18
0506	18	18	18	18	18	18
0509	18	18	18	18	18	18
0511	18	18	18	18	17	17.8
0512	18	18	18	18	17	17.8
0513	18	18	18	18	17	17.8
0714	18	18	18	18	18	18
0803	17	18	18	18	18	17.8
0805	13	14	13	13	13	13.2
0819	18	18	18	18	18	18
1000	17	17	16	16	17	16.6
1007	18	18	18	18	17	17.8
1012	18	18	18	18	18	18
1101	18	18	18	18	18	18
1102	18	18	18	18	18	18
1204	18	18	17	17	17	17.4
1612	17	17	17	17	15	16.6
3131	18	18	17.8	17.4	18	17.84
3132	18	18	18	18	18	18
9404	17	18	18	18	18	17.8

used because the CWE per regime spanned all months and years within the PoR. The result was a dataset of CWE frequencies per year for 42 towers that were calculated with respect to the PoR, WS months, and synoptic flow regime.

3.5 Contour Maps

The final step was to generate maps for the geographic distribution of CWE frequencies with respect to the categorical datasets. ArcMap 10.5 was utilized for map generation. Within the mapping process there were three stages for creating each map: 1) the frequency dataset was imported, 2) data was interpolated, and 3) the interpolation raster was contoured.

The first step to map the frequencies was to import and overlay the data onto a base map. The maps created for this research were generated with ArcGIS® software by Esri. The ArcGIS® World Light Gray Canvas Base Map was chosen as the base map because it provided a neutral background which allowed the geographic context to be emphasized. As mentioned before, there were six physical towers for which there were two sensor suites. To keep both values at the tower location would have complicated interpolation and contouring. To simplify the process the highest CWE frequency of the co-located TIDs was retained for the location. In most cases the values were similar.

Next, a natural neighbor technique was used to interpolate a raster surface from the tower points. This technique used a subset of samples that surrounded the query point and weighted the subset based on comparable areas to interpolate value. In this case the query points were the CWE frequencies at each tower.

The third step in mapping was to create contours based on the natural neighbor raster image. A contour interval of one CWE per year was used for the PoR. The maps for the WS months and flow regimes were each contoured at an interval of 0.2 CWE per year allow for sample comparisons and analysis.

3.6 Bootstrap Confidence Interval

There was some difference noted between the subcategory ranges of CWE frequency; this gave an indication that there were some differences in the spread. The spread within a distribution is captured by standard deviation. The bootstrap statistical technique is applied to the data and resulted in confirmation that there were differences in the subcategory spreads.

The true standard deviation cannot be known from the finite sample of 42 CWE frequencies per subcategory. To estimate the true standard deviation a bootstrap confidence interval is computed for each subcategory (Orloff and Bloom 2014). A bootstrap confidence interval is a range computed to estimate the unknown parameter, here the standard deviation about the mean, with a given confidence level. The bootstrap method is roughly founded on the law of large numbers which in summary states that with enough data the observed distribution is a good approximation of the true distribution. Bootstrap gives a decent estimate of true standard deviation through the use of resampling. To resample is to sample with replacement from the observed data set. The CWE frequency database is normalized and then the bootstrap technique is executed with a resample of 100,000. This is performed to estimate the standard deviation about

the mean for each subcategory with a confidence interval of 90% as seen in Figure 8 and Figure 9.

These figures show plots of bootstrapped confidence intervals of standard deviation about the mean for each normalized subcategory of CWE frequencies per year. The vertical axis represents the standard deviation about the mean and the horizontal axis represent the subcategories. For each plot within Figures 8 and 9 it may be said with that the true standard deviation is within the error bars 90% certainty. A lower standard deviation indicates a more uniform distribution or less varied dataset (Penn State 2017). Higher standard deviation indicates a greater distribution or more varied dataset of CWE frequency.

Error bars are used on plots to signify uncertainty in a reported measurement and to graphically represent data variability (Penn State 2017). They give an idea of how far a true value may be from an observed value. The position of error bars relative to other subcategories allows for comparison of the distribution spreads. Meaning that if there is no overlap in the error bars between subcategories then the spread of CWE frequencies between those compared is statistically significant with 90% confidence. Overlap of error bars means the groups are not statistically significant. When compared datasets are statistically significant it means that there is a real difference in the spreads of frequency and that the differences are not due to sampling error, which is the difference between a sample statistic used to estimate a population parameter and the true but unknown value of the parameter. We cannot know the true value from a finite sample.

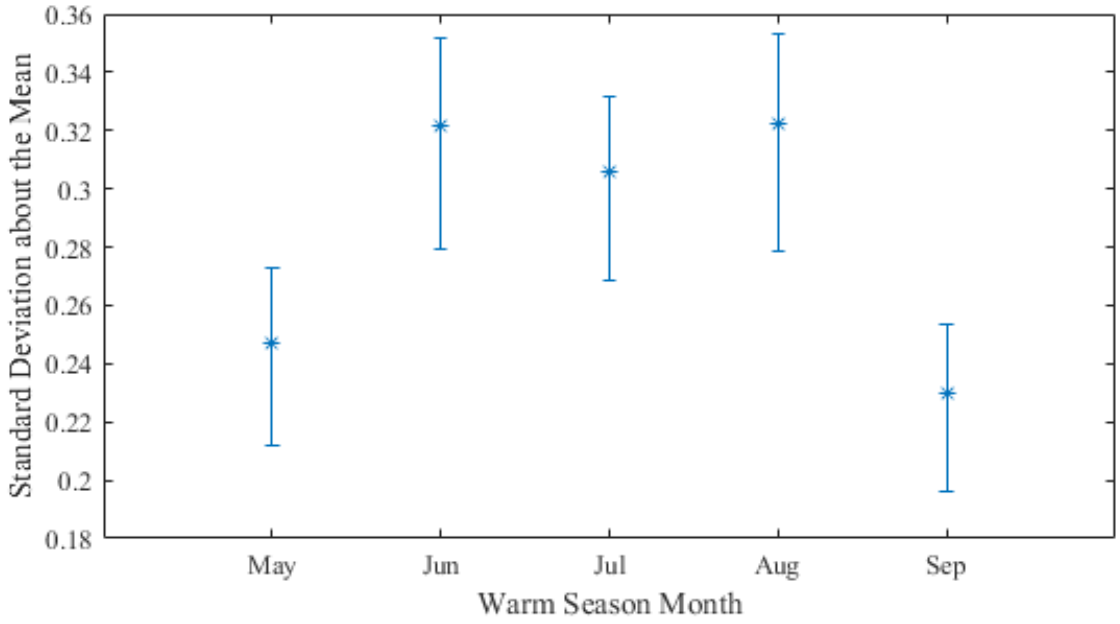

Figure 8. Bootstrapped confidence intervals of 90% by month. Standard deviation about the mean for the normalized CWE frequencies of 100,000 resamples for each warm-season month.

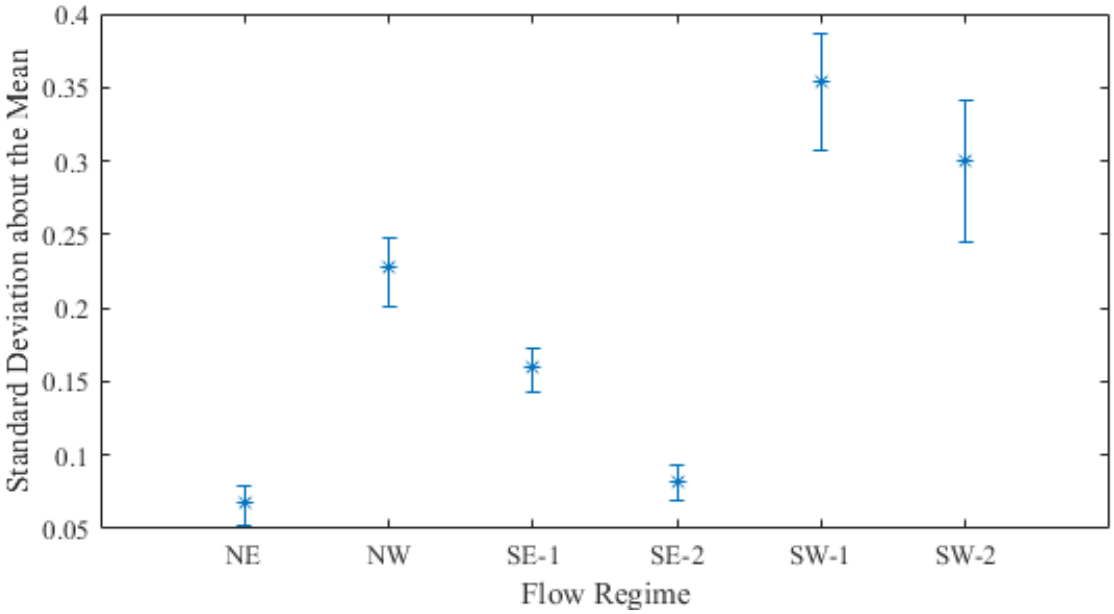

Figure 9. Bootstrapped confidence intervals of 90% as in Figure 8, except with respect to flow regime.

IV. Analysis and Results

This chapter presents and analyzes the CWE frequency per year for each TID with respect to the categories of PoR, WS months, and synoptic flow regimes. It is apparent that the CWE frequencies vary across the AoS for each category. Additionally, it is evident that within the WS months the frequency varies seasonally. There is a distinct pattern that emerges in the PoR and it is mimicked in each WS month and in the regimes of westerly component. The pattern is most pronounced for the subcategories of higher convective activity compared to those of lesser convection. The TIDs are stratified by their geographic location as seen in Figure 10. This allows for a simplified discussion of the overall patterns that are yielded. The mainland is the western most region and is marked in gold. The coastal area is marked in light blue and is east of Mosquito Lagoon, Merritt Island, and the Banana River. The central and Merritt Island area is flanked by the mainland and coastal areas; it includes the Indian River and Banana River/Lagoon. The most prominent geographic distribution of CWE frequency that emerges from the datasets is of strong coastal maxima with minima that are generally inland. Contour mapping of the CWE frequency per year supports this finding (se Figures 11-22).

4.1 Analysis of CWE Frequencies for the PoR

First, the CWE frequency per year for each tower with respect to the PoR is presented (Table 8). This table is a collection of CWE frequencies for the PoR and WS months. The far-left column lists the TIDs in numerical order; 12 TIDs are color filled to match their co-located sensor suites. Next are the columns of CWE frequencies per year for

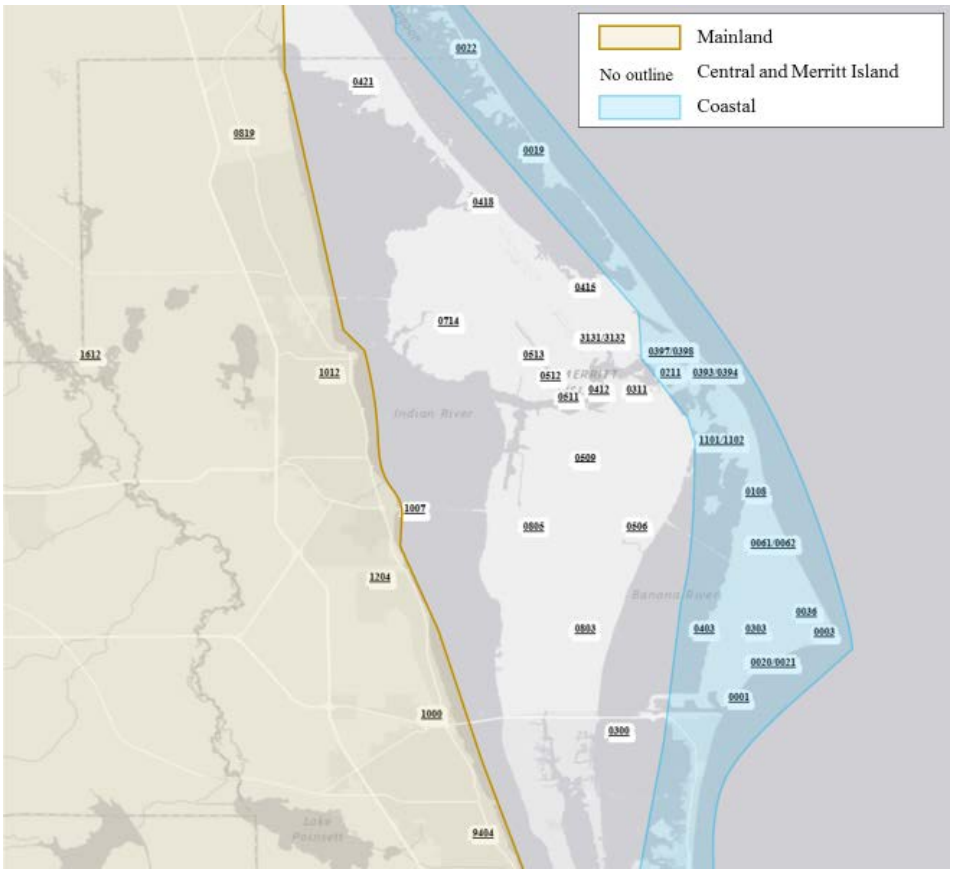

Figure 10. Geographic stratification of tower location.

each WS month, and the last column is the PoR data. The frequency data in Table 8 is conditionally formatted with color data bars. These bars represent the value within the cell compared to the other cells within the subcategory; therefore, the higher the value, the longer the bar. For example, in Table 8 the highest frequency for the PoR is 7.85 at tower 3131; this cell has the longest bar in the dataset. The lowest frequency for the PoR is 0.17 at tower 1204; this cell has the shortest bar in the column. It is evident by visual inspection that the frequencies for the PoR and WS months vary across the AoS. Additionally, it is noted that the pattern created by the PoR data bars is reflected in each monthly dataset. This gives the impression that the general areas of high and low frequencies are similar to those for the PoR.

Table 8. CWE frequency per year for each TID. The TID cells colored as in Figure 3. The frequency cells are conditionally formatted with red color data bars.

TID	May	Jun	Jul	Aug	Sep	PoR
0001	0.17	0.67	0.56	0.56	0.29	2.25
0003	0.41	0.76	1.00	0.82	0.35	3.35
0019	0.29	1.35	1.38	0.94	0.31	4.28
0020	0.59	1.65	1.65	1.71	0.69	6.26
0021	0.53	2.00	1.65	1.65	0.61	6.40
0022	0.56	1.39	2.28	1.28	0.27	5.92
0036	0.20	0.30	0.30	0.70	0.20	1.70
0061	0.72	2.06	1.83	1.56	0.72	6.89
0062	0.61	1.61	1.67	1.33	0.56	5.78
0108	0.29	1.22	0.72	0.83	0.28	3.37
0211	0.33	1.11	1.00	0.89	0.33	3.67
0300	0.44	1.72	1.28	1.22	0.28	4.94
0303	0.17	0.22	0.17	0.11	0.06	0.72
0311	0.28	0.94	1.11	0.72	0.17	3.22
0393	0.53	0.88	0.59	0.76	0.19	2.98
0394	0.71	0.88	0.94	0.88	0.25	3.66
0397	0.27	1.07	0.80	0.87	0.21	3.24
0398	0.40	1.07	1.00	0.60	0.23	3.36
0403	0.44	1.06	0.72	0.83	0.33	3.39
0412	0.06	0.61	0.44	0.44	0.11	1.67
0415	0.11	0.50	0.44	0.44	0.06	1.56
0418	0.11	0.28	0.50	0.44	0.06	1.39
0421	0.67	1.22	1.83	1.22	0.56	5.50
0506	0.11	0.56	0.61	0.28	0.28	1.83
0509	0.17	0.83	0.44	0.28	0.17	1.89
0511	0.28	0.89	0.94	0.94	0.24	3.31
0512	0.11	0.50	0.72	0.72	0.18	2.25
0513	0.11	1.06	0.83	0.72	0.06	2.81
0714	0.28	1.11	1.06	0.94	0.11	3.50
0803	0.06	0.44	0.44	0.17	0.06	1.18
0805	0.08	0.14	0.31	0.08	0.00	0.61
0819	0.11	0.11	0.17	0.22	0.00	0.61
1000	0.24	0.41	0.50	0.63	0.06	1.81
1007	0.39	1.50	0.89	0.94	0.24	3.99
1012	0.00	0.06	0.17	0.00	0.00	0.22
1101	0.94	2.61	1.72	1.56	0.72	7.56
1102	0.89	2.28	1.50	1.61	0.78	7.06
1204	0.00	0.11	0.06	0.00	0.00	0.17
1612	0.29	0.71	0.71	0.53	0.07	2.35
3131	0.56	2.28	2.08	2.30	0.67	7.85
3132	0.72	2.06	2.11	2.17	0.61	7.67
9404	0.12	0.39	0.28	0.50	0.06	1.35

The similarity is quantified in Table 9 by the statistical values drawn from Table 8. These values for the PoR show a frequency range of 0.17 to 7.85 CWE per year. The average CWE per year for the PoR was 3.42. The maximum occurred at TID 3131 and was followed closely by the co-located TID 3132 with a value of 7.67 CWE per year; the tower is located within three miles of the coast in the Central and Merritt Island area. The lowest frequency is 0.17 CWE per year and occurs at the mainland TID of 1204.

4.2 Analysis of CWE Frequencies for WS Months

The second category that is analyzed for CWE frequencies is WS months. There is a distinct difference in the average frequency per year for May and September compared to June, July, and August. May and September are considered seasonally as transition months for which less convective activity occurs. These seasonal descriptors are well established in numerous studies of different data and time periods (Roeder, Personal Communication December 8, 2017). June, July, and August are the months of

Table 9. Statistical values for CWE frequencies per WS month and PoR.

	May (TID)	Jun (TID)	Jul (TID)	Aug (TID)	Sep (TID)	PoR (TID)
Maxima	**0.94** (1101)	**2.61** (1101)	**2.28** (0022)	**2.3** (3131)	**0.78** (1102)	**7.85** (3131)
Minima	**0.00** (1012, 1204)	**0.06** (1012)	**0.06** (1204)	**0.00** (1012, 1204)	**0.00** (0805, 0819, 1012, 1204)	**0.17** (1204)
Average	**0.34**	**1.01**	**0.94**	**0.84**	**0.27**	**3.42**

peak convection. This may be noted from Table 10 which is compiled of information gathered in this study and from the OCDS-II. It is evident from this table that of all WS months July generally has the most convective activity. This is concluded for July because it has the greatest mean thunderstorm days for KXMR and Patrick Air Force Base (KCOF); and matches the highest thunderstorm days mean for NASA Shuttle Landing Facility on KSC (KTTS) in August. June, July, and August have comparable CP and CWE. July and August have a CP frequency of 27% and that of June is 22%. July stands out with a CWE frequency of 30% and is followed by June and August with 25% and 26%, respectively.

The statistical frequency values for the peak month are comparable (Table 9). June has the highest maximum frequency of 2.61 CWE per year of all towers for any month. This maximum occurred at the coastal tower 1101. Additionally, it has the

Table 10. Summary of statistical values for convective parameters.

WS Month	TS Days Mean (KTTS)*	TS Days Mean (KXMR)*	TS Days Mean (KCOF)*	CP Count	CP Frequency	CWE Count	CWE Frequency
May	5	5	6	107	9%	44	10%
Jun	12	10	13	253	22%	108	25%
Jul	15	13	15	303	27%	130	30%
Aug	15	11	13	304	27%	115	26%
Sep	8	8	9	168	15%	43	10%

* (14 WS 2017)

highest average frequency of 1.01 CWE per year. Its minimum frequency is 0.06 and is recorded for the mainland tower of 1012. The minimum frequency for July is the same as June's and occurs at the mainland tower of 1204. The average CWE frequencies for July and August closely follow that of June with values of 0.94 and 0.84 CWE per year, respectively. The range of values for July and August are also comparable with ranges of 0.06 to 2.28 CWE per year and 0.00 to 2.30 CWE per year, respectively. The tower locations for frequency maxima are in the coastal and Merritt Island areas. The minima occur at mainland towers. The average tower frequencies for the transition months are comparable at 0.34 CWE per year for May and 0.27 CWE per year for September. The range of values for these months are 0.00 to 0.94 CWE per year and 0.00 to 0.78 CWE per year, respectively.

After the statistical data analysis was accomplished, the CWE frequencies per year were sorted in descending order for each WS month and PoR as seen in Table 11. The frequency cells of this table were color filled according to geographic stratification as was described for Figure 10. The cell colors for the mainland TIDs were gold; those in the central and Merritt Island area were colored white; and cells for the coastal areas were filled with light blue. From Table 11 it may be quickly noted that the highest frequencies for the PoR are generally associated with coastal and central towers. The top five values of CWE frequencies per year for the PoR generally occurred near the coast while the lowest values are found over mainland locations. This distinctive pattern was mimicked by each of the WS months and is even more apparent when overlaid on a map.

Table 11. CWE frequency per year for each TID with respect to WS month. The TID cells colored as in Figure 3. The frequency cells are color filled to denote geographic location as stratified in Figure 10. The cell colors for the mainland TIDs are gold; those in the central and Merritt Island area are white; and cells for the coastal areas are light blue.

TID	May		Tower	Jun		Tower	Jul		Tower	Aug		Tower	Sep		Tower	PoR
1101	0.94		1101	2.61		0022	2.28		3131	2.30		1102	0.78		3131	7.85
1102	0.89		3131	2.28		3132	2.11		3132	2.17		1101	0.72		3132	7.67
3132	0.72		1102	2.28		3131	2.08		**0020**	1.71		0061	0.72		1101	7.56
0061	0.72		3132	2.06		0061	1.83		**0021**	1.65		**0020**	0.69		1102	7.06
0394	0.71		0061	2.06		0421	1.83		1102	1.61		3131	0.67		0061	6.89
0421	0.67		**0021**	2.00		1101	1.72		1101	1.56		3132	0.61		**0021**	6.40
0062	0.61		0300	1.72		0062	1.67		0061	1.56		**0021**	0.61		**0020**	6.26
0020	0.59		**0020**	1.65		**0021**	1.65		0062	1.33		0062	0.56		0022	5.92
3131	0.56		0062	1.61		**0020**	1.65		0022	1.28		0421	0.56		0062	5.78
0022	0.56		1007	1.50		1102	1.50		0421	1.22		0003	0.35		0421	5.50
0021	0.53		0022	1.39		0019	1.38		0300	1.22		0211	0.33		0300	4.94
0393	0.53		0019	1.35		0300	1.28		1007	0.94		0403	0.33		0019	4.28
0300	0.44		0421	1.22		0311	1.11		0714	0.94		0019	0.31		1007	3.99
0403	0.44		0108	1.22		0714	1.06		0511	0.94		0001	0.29		0211	3.67
0003	0.41		0714	1.11		0211	1.00		0019	0.94		0300	0.28		0394	3.66
0398	0.40		0211	1.11		0398	1.00		0211	0.89		0108	0.28		0714	3.50
1007	0.39		0398	1.07		0003	1.00		0394	0.88		0506	0.28		0403	3.39
0211	0.33		0397	1.07		0511	0.94		0397	0.87		0022	0.27		0108	3.37
0019	0.29		0513	1.06		0394	0.94		0403	0.83		0394	0.25		0398	3.36
0108	0.29		0403	1.06		1007	0.89		0108	0.83		1007	0.24		0003	3.35
1612	0.29		0311	0.94		0513	0.83		0003	0.82		0511	0.24		0511	3.31
0714	0.28		0511	0.89		0397	0.80		0393	0.76		0398	0.23		0397	3.24
0511	0.28		0394	0.88		0403	0.72		0311	0.72		0397	0.21		0311	3.22
0311	0.28		0393	0.88		0108	0.72		0513	0.72		0036	0.20		0393	2.98
0397	0.27		0509	0.83		0512	0.72		0512	0.72		0393	0.19		0513	2.81
1000	0.24		0003	0.76		1612	0.71		0036	0.70		0512	0.18		1612	2.35
0036	0.20		1612	0.71		0506	0.61		1000	0.63		0311	0.17		0001	2.25
0001	0.17		0001	0.67		0393	0.59		0398	0.60		0509	0.17		0512	2.25
0509	0.17		0412	0.61		0001	0.56		0001	0.56		0714	0.11		0509	1.89
0303	0.17		0506	0.56		1000	0.50		1612	0.53		0412	0.11		0506	1.83
9404	0.12		0512	0.50		0418	0.50		9404	0.50		1612	0.07		1000	1.81
0513	0.11		0415	0.50		0509	0.44		0412	0.44		0513	0.06		0036	1.70
0512	0.11		0803	0.44		0412	0.44		0415	0.44		1000	0.06		0412	1.67
0506	0.11		1000	0.41		0415	0.44		0418	0.44		0415	0.06		0415	1.56
0415	0.11		9404	0.39		0803	0.44		0509	0.28		0418	0.06		0418	1.39
0418	0.11		0036	0.30		0805	0.31		0506	0.28		9404	0.06		9404	1.35
0819	0.11		0418	0.28		0036	0.30		0819	0.22		0803	0.06		0803	1.18
0805	0.08		0303	0.22		9404	0.28		0803	0.17		0303	0.06		0303	0.72
0803	0.06		0805	0.14		0303	0.17		0303	0.11		0819	0.00		0819	0.61
0412	0.06		1204	0.11		0819	0.17		0805	0.08		0805	0.00		0805	0.61
1012	0.00		0819	0.11		1012	0.17		1012	0.00		1012	0.00		1012	0.22
1204	0.00		1012	0.06		1204	0.06		1204	0.00		1204	0.00		1204	0.17

4.3 Analysis of CWE Frequencies for Synoptic Flow

The CWE frequency with respect to the synoptic flow is the last category analyzed. The regimes are described by the subcategories westerly and easterly because there is a distinct difference in the level of convective activity between the two and the difference between their frequency spreads is noticeable as indicated by the applied bootstrap technique (Fig. 9). Some regimes have more convection than others. Table 12 presents CPs and CWEs counts and occurrences per regime for the PoR. The blue and green data bars in the cells allow for a quick analysis of how a cell value compares to the other values within the datasets; SW-1 and SW-2 are distinctly more active as noted by the higher CP and CWE counts.

A majority (63%) of CPs occur under a flow of westerly component. CPs occur at a 25% occurrence under easterly regimes. While the subcategories of "Other" and "Missing" account for 12% of occurrences. A majority (78%) of CWEs occur under westerly regimes. It is seen that CWE are relatively uncommon under easterly

Table 12. Count of CPs and CWEs per flow regime. The blue and green data bars in the cells allow for a quick analysis of how a cell value compares to the other values within the datasets.

Regime	CP Count	CP Frequency	CWE Count	CWE Frequency
SW-1	220	0.19	126	0.29
SW-2	380	0.33	172	0.39
NW	110	0.10	46	0.10
SE-1	148	0.13	27	0.06
SE-2	80	0.07	17	0.04
NE	60	0.05	7	0.02
Other	115	0.10	37	0.08
Missing	22	0.02	8	0.02
Total	1135		440	

component flows (12%) and are least common under “Other” and “Missing” flows (10%). The subcategory of “Missing” is defined by the fact that (synoptic data to determine the flow regime is missing from the archive (Lericos 2002; Lambert 2007). “Other” is based on an undefined position of the subtropical ridge. There are 115 CPs and 37 CWEs that are archived under these regimes; this accounts for 10% of CPs and 8% of CWEs. The “Other” and “Missing” regimes are not further analyzed in this research because it is deemed insignificant for operational use.

The counts of CP and CWE indicate that SW-1 and SW-2 are the regimes of greatest convective activity (Table 12). SW-2 has the greatest occurrence of CPs and CWEs at 33% and 39%, respectively. SW-1 has the second highest occurrence of CPS and CWEs at 19% and 29%, respectively. NW flow has 10% for both CP and CWE frequencies. Compared to NW, SE-1 has a slightly higher CP occurrence of 13% but a lower CWE frequency of 6%. The CP occurrence for SE-2 and NE were 7% and 5%, respectively. Both regimes have low CWE frequencies of 4% and 2%.

The CWE frequencies per year for the regimes is compiled into Table 13. The data for the PoR is included for comparison. The far-left column listed the TIDs in numerical order; 12 TIDs are color filled to match their co-located sensor suites. The next columns are of CWE frequencies per flow, and the last column is for the PoR frequencies. The frequency columns of the table are conditionally formatted with color data bars as described for Table 8. The table is sorted in numerically by TID. It is

Table 13. Tower CWE frequency per year with respect to synoptic regime. TIDs are color coded as in Table 3 and the frequency cells are conditionally formatted with color data bars as in Table 8.

TID	SW-1	SW-2	NW	SE-1	SE-2	NE	PoR
0001	0.84	0.79	0.17	0.11	0.11	0.00	2.25
0003	0.82	0.65	0.65	0.29	0.29	0.06	3.35
0019	1.45	1.57	0.48	0.30	0.18	0.00	4.28
0020	1.87	2.28	0.64	0.53	0.29	0.18	6.26
0021	2.27	2.15	0.70	0.47	0.23	0.12	6.40
0022	1.67	2.59	0.80	0.40	0.00	0.06	5.92
0036	0.10	0.30	0.60	0.20	0.20	0.10	1.70
0061	2.06	2.33	0.83	0.39	0.11	0.28	6.89
0062	1.78	2.06	0.67	0.39	0.11	0.17	5.78
0108	1.29	1.29	0.51	0.06	0.00	0.00	3.37
0211	1.50	1.11	0.44	0.06	0.11	0.11	3.67
0300	1.50	1.78	0.72	0.33	0.17	0.00	4.94
0303	0.28	0.22	0.11	0.06	0.00	0.06	0.72
0311	0.83	1.61	0.44	0.11	0.06	0.06	3.22
0393	1.01	1.01	0.48	0.12	0.12	0.12	2.98
0394	1.34	1.34	0.61	0.06	0.06	0.12	3.66
0397	1.15	1.22	0.34	0.27	0.07	0.07	3.24
0398	0.89	1.51	0.41	0.27	0.07	0.07	3.36
0403	1.17	1.11	0.44	0.11	0.17	0.06	3.39
0412	0.39	0.78	0.22	0.06	0.00	0.06	1.67
0415	0.44	0.72	0.28	0.00	0.00	0.00	1.56
0418	0.28	0.61	0.28	0.00	0.06	0.00	1.39
0421	1.50	2.06	0.72	0.50	0.11	0.00	5.50
0506	0.56	0.56	0.33	0.11	0.00	0.00	1.83
0509	0.72	0.67	0.28	0.06	0.00	0.00	1.89
0511	1.18	1.24	0.51	0.11	0.06	0.00	3.31
0512	0.51	1.07	0.28	0.11	0.06	0.00	2.25
0513	1.24	0.79	0.34	0.28	0.06	0.00	2.81
0714	1.06	1.50	0.44	0.22	0.06	0.00	3.50
0803	0.45	0.51	0.06	0.06	0.00	0.00	1.18
0805	0.00	0.23	0.38	0.00	0.00	0.00	0.61
0819	0.11	0.22	0.22	0.00	0.00	0.00	0.61
1000	0.54	0.72	0.18	0.12	0.00	0.00	1.81
1007	1.18	1.40	0.62	0.34	0.22	0.06	3.99
1012	0.00	0.00	0.11	0.06	0.00	0.00	0.22
1101	2.67	2.67	0.89	0.39	0.11	0.22	7.56
1102	2.44	2.61	0.83	0.33	0.11	0.11	7.06
1204	0.00	0.06	0.06	0.06	0.00	0.00	0.17
1612	0.42	1.08	0.36	0.24	0.06	0.00	2.35
3131	2.63	3.36	0.67	0.45	0.17	0.06	7.85
3132	2.39	3.56	0.61	0.44	0.11	0.06	7.67
9404	0.28	0.62	0.22	0.06	0.06	0.00	1.35

evident by visual inspection that within each regime the CWE frequencies are varied across the AoS. The data bar patterns of SW-1 and SW-2 are visually most like that of the PoR. Within the westerly regimes it is noted that the NW flow was slightly different from the two very similar southwest flows. The patterns for NW and SE-1 are somewhat similar to the PoR. SE-2 and NE are visually dissimilar to that of the PoR.

Table 14 shows the maxima, minima, and average CWE frequency per year for each regime from the data in Table 13. The values for SW-1 and SW-2 are comparable. SW-2 has the largest range of frequency, zero to 3.56 CWE per year, and highest average frequency of 1.28 CWE per year. The minimum and maximum frequencies occur at the mainland tower of 1012 and a near coastal tower of 3132 (Merritt Island). The second highest values are recorded for SW-1. This regime has a frequency range of zero to 2.67 events per year; and an average frequency of 1.07. The minimum occurs at three towers (and locations): 0805 (central), 1012 (mainland), and 1204 (mainland). The maximum frequency for SW-1 occurs at the coastal tower of 1101. The third highest statistical values of minimum, maximum, and average frequency were found for the NW regime; they were 0.06, 0.89, and 0.45, respectively. The minimum occurs at two locations which are 0803 (central) and 1204 (mainland); the maximum occurs at the coastal tower of 1101. The average, maxima, and minima frequency details for the easterly regimes all fell below one. All had minimum CWE frequencies of zero events per year that occur at multiple towers across the AoS. The CWE maximums were 0.53 (0020 coastal), 0.29 (0003 and 0020, coastal), and 0.28 (0061 coastal) events per year, respectively for SE-1, SE-2, and NE; all occur at coastal towers as indicated by the color coding of Table 13. The average frequencies, respectively, were 0.20, 0.09, and 0.05.

Table 14. Statistical values of CWE frequencies with respect to flow regime.

	SW-1 (TID)	SW-2 (TID)	NW (TID)	SE-1 (TID)	SE-2 (TID)	NE (TID)
Maxima	2.67 (1101)	3.56 (3132)	0.89 (1101)	0.53 (0020)	0.29 (0003, 0020)	0.28 (0061)
Minima	0.00 (0805, 1012, 1204)	0.00 (1012)	0.06 (0803, 1204)	0.00 (0415, 0418, 0805, 0819)	0.00 (0022, 0108, 0303, 0412, 0415, 0506, 0509, 0803, 0805, 0819, 1000, 1012, 1204)	0.00 (0001, 0019, 0108, 0300, 0415, 0418, 0421, 0506, 0509, 0511, 0512, 0513, 0714, 0803, 0805, 0819, 1000, 1012, 1204, 1612, 9404)
Average	1.07	1.28	0.45	0.20	0.09	0.05

4.4 CWE Frequency Contour Maps

Mapping allows for visualization of the geographic distribution of CWE frequencies and interpolation of occurrence between towers. For purposes of contour mapping the co-located TIDs are accounted for as one location and the higher of the two CWE frequencies is retained as seen in Table 15 and 16. This results in the plot of 36 data points for each map generated. This section describes details for the maps of CWE distributions generated for the PoR, the WS months, and six synoptic flow regimes.

From the datasets and contoured maps, it is noted that the general area of towers with the highest values are in the coastal region and the location of the lowest values differs depending on the subcategory. The towers of lowest values for the WS months and westerly flow regimes generally followed the same pattern as the PoR. For easterly flow regimes the location of towers with the lowest values is scattered across the AoS. The tables of CWE frequencies are sorted in descending order and are color coded like

Table 11. This allows for quick analysis of the general areas of highest and lowest frequencies. The towers of highest and lowest values that match those of the PoR are underlined. The maps are marked with red and green triangle for the highest and lowest values, respectively.

Table 15. CWE frequency per year for the 36 tower locations with respect to the WS months and PoR. The co-located TIDs in vibrant hues are accounted for as one location. The greater of the two frequencies is retained for mapping. The frequency cells are color filled as in Table 11.

Tower	May	Tower	Sep	Tower	Jun	Tower	Jul	Tower	Aug	Tower	PoR
1101/1102	0.94	1101/1102	0.78	1101/1102	2.61	0022	2.28	3131/3132	2.30	3131/3132	7.85
0061/0062	0.72	0061/0062	0.72	3131/3132	2.28	3131/3132	2.11	0020/0021	1.71	1101/1102	7.56
3131/3132	0.72	0020/0021	0.69	0061/0062	2.06	0421	1.83	1101/1102	1.61	0061/0062	6.89
0393/0394	0.71	3131/3132	0.67	0020/0021	2.00	0061/0062	1.83	0061/0062	1.56	0020/0021	6.40
0421	0.67	0421	0.56	0300	1.72	1101/1102	1.72	0022	1.28	0022	5.92
0020/0021	0.59	0003	0.35	1007	1.50	0020/0021	1.65	0300	1.22	0421	5.50
0022	0.56	0211	0.33	0022	1.39	0019	1.38	0421	1.22	0300	4.94
0300	0.44	0403	0.33	0019	1.35	0300	1.28	0511	0.94	0019	4.28
0403	0.44	0019	0.31	0108	1.22	0311	1.11	0714	0.94	1007	3.99
0003	0.41	0001	0.29	0421	1.22	0714	1.06	1007	0.94	0211	3.67
0397/0398	0.40	0108	0.28	0211	1.11	0003	1.00	0019	0.94	0393/0394	3.66
1007	0.39	0300	0.28	0714	1.11	0211	1.00	0211	0.89	0714	3.50
0211	0.33	0506	0.28	0397/0398	1.07	0397/0398	1.00	0393/0394	0.88	0403	3.39
0019	0.29	0022	0.27	0403	1.06	0511	0.94	0397/0398	0.87	0108	3.37
0108	0.29	0393/0394	0.25	0513	1.06	0393/0394	0.94	0108	0.83	0397/0398	3.36
1612	0.29	0511	0.24	0311	0.94	1007	0.89	0403	0.83	0003	3.35
0311	0.28	1007	0.24	0511	0.89	0513	0.83	0003	0.82	0511	3.31
0511	0.28	0397/0398	0.23	0393/0394	0.88	0108	0.72	0311	0.72	0311	3.22
0714	0.28	0036	0.20	0509	0.83	0403	0.72	0512	0.72	0513	2.81
1000	0.24	0512	0.18	0003	0.76	0512	0.72	0513	0.72	1612	2.35
0036	0.20	0311	0.17	1612	0.71	1612	0.71	0036	0.70	0001	2.25
0001	0.17	0509	0.17	0001	0.67	0506	0.61	1000	0.63	0512	2.25
0303	0.17	0412	0.11	0412	0.61	0001	0.56	0001	0.56	0509	1.89
0509	0.17	0714	0.11	0506	0.56	0418	0.50	1612	0.53	0506	1.83
9404	0.12	1612	0.07	0415	0.50	1000	0.50	9404	0.50	1000	1.81
0415	0.11	0513	0.06	0512	0.50	0412	0.44	0412	0.44	0036	1.70
0418	0.11	1000	0.06	0803	0.44	0415	0.44	0415	0.44	0412	1.67
0506	0.11	0303	0.06	1000	0.41	0509	0.44	0418	0.44	0415	1.56
0512	0.11	0415	0.06	9404	0.39	0803	0.44	0506	0.28	0418	1.39
0513	0.11	0418	0.06	0036	0.30	0805	0.31	0509	0.28	9404	1.35
0819	0.11	0803	0.06	0418	0.28	0036	0.30	0819	0.22	0803	1.18
0805	0.08	9404	0.06	0303	0.22	9404	0.28	0803	0.17	0303	0.72
0803	0.06	0805	0.00	0805	0.14	0303	0.17	0303	0.11	0819	0.61
0412	0.06	0819	0.00	0819	0.11	0819	0.17	0805	0.08	0805	0.61
1012	0.00	1012	0.00	1204	0.11	1012	0.17	1012	0.00	1012	0.22
1204	0.00	1204	0.00	1012	0.06	1204	0.06	1204	0.00	1204	0.17

Table 16. CWE frequency per year with respect to flow regime and PoR. The towers cells and the frequency cells are color filled as in Table 15 and Table 11, respectively.

Tower	SW-1	Tower	SW-2	Tower	NW	Tower	SE-1	Tower	SE-2	Tower	NE	Tower	PoR
1101/1102	2.67	3131/3132	3.56	1101/1102	0.89	0020/0021	0.53	0003	0.29	0061/0062	0.28	3131/3132	7.85
3131/3132	2.63	1101/1102	2.67	0061/0062	0.83	0421	0.50	0020/0021	0.29	1101/1102	0.22	1101/1102	7.56
0020/0021	2.27	0022	2.59	0022	0.80	3131/3132	0.45	1007	0.22	0020/0021	0.18	0061/0062	6.89
0061/0062	2.06	0061/0062	2.33	0300	0.72	0022	0.40	0036	0.20	0393/0394	0.12	0020/0021	6.40
0022	1.67	0020/0021	2.28	0421	0.72	0061/0062	0.39	0019	0.18	0211	0.11	0022	5.92
0211	1.50	0421	2.06	0020/0021	0.70	1101/1102	0.39	3131/3132	0.17	0036	0.10	0421	5.50
0300	1.50	0300	1.78	3131/3132	0.67	1007	0.34	0300	0.17	0397/0398	0.07	0300	4.94
0421	1.50	0311	1.61	0003	0.65	0300	0.33	0403	0.17	0003	0.06	0019	4.28
0019	1.45	0019	1.57	1007	0.62	0019	0.30	0393/0394	0.12	0022	0.06	1007	3.99
0393/0394	1.34	0397/0398	1.51	0393/0394	0.61	0003	0.29	0001	0.11	1007	0.06	0211	3.67
0108	1.29	0714	1.50	0036	0.60	0513	0.28	0061/0062	0.11	3131/3132	0.06	0393/0394	3.66
0513	1.24	1007	1.40	0108	0.51	0397/0398	0.27	0211	0.11	0303	0.06	0714	3.50
0511	1.18	0393/0394	1.34	0511	0.51	1612	0.24	0421	0.11	0311	0.06	0403	3.39
1007	1.18	0108	1.29	0019	0.48	0714	0.22	1101/1102	0.11	0403	0.06	0108	3.37
0403	1.17	0511	1.24	0211	0.44	0036	0.20	0397/0398	0.07	0412	0.06	0397/0398	3.36
0397/0398	1.15	0211	1.11	0311	0.44	1000	0.12	1612	0.06	0001	0.00	0003	3.35
0714	1.06	0403	1.11	0403	0.44	0393/0394	0.12	0511	0.06	0019	0.00	0511	3.31
0001	0.84	1612	1.08	0714	0.44	0001	0.11	0512	0.06	0108	0.00	0311	3.22
0311	0.83	0512	1.07	0397/0398	0.41	0511	0.11	0513	0.06	0300	0.00	0513	2.81
0003	0.82	0001	0.79	0805	0.38	0512	0.11	9404	0.06	0415	0.00	1612	2.35
0509	0.72	0513	0.79	1612	0.36	0311	0.11	0311	0.06	0418	0.00	0001	2.25
0506	0.56	0412	0.78	0513	0.34	0403	0.11	0418	0.06	0421	0.00	0512	2.25
1000	0.54	1000	0.72	0506	0.33	0506	0.11	0714	0.06	0506	0.00	0509	1.89
0512	0.51	0415	0.72	0512	0.28	1204	0.06	0022	0.00	0509	0.00	0506	1.83
0803	0.45	0509	0.67	0415	0.28	0108	0.06	0108	0.00	0511	0.00	1000	1.81
0415	0.44	0003	0.65	0418	0.28	0803	0.06	0303	0.00	0512	0.00	0036	1.70
1612	0.42	9404	0.62	0509	0.28	9404	0.06	0412	0.00	0513	0.00	0412	1.67
0412	0.39	0418	0.61	9404	0.22	0211	0.06	0415	0.00	0714	0.00	0415	1.56
9404	0.28	0506	0.56	0412	0.22	0303	0.06	0506	0.00	0803	0.00	0418	1.39
0303	0.28	0803	0.51	0819	0.22	0412	0.06	0509	0.00	0805	0.00	9404	1.35
0418	0.28	0036	0.30	1000	0.18	0509	0.06	0803	0.00	0819	0.00	0803	1.18
0819	0.11	0805	0.23	0001	0.17	1012	0.06	0805	0.00	1000	0.00	0303	0.72
0036	0.10	0303	0.22	0303	0.11	0415	0.00	0819	0.00	1012	0.00	0819	0.61
0805	0.00	0819	0.22	1012	0.11	0418	0.00	1000	0.00	1204	0.00	0805	0.61
1012	0.00	1204	0.06	1204	0.06	0805	0.00	1012	0.00	1612	0.00	1012	0.22
1204	0.00	1012	0.00	0803	0.06	0819	0.00	1204	0.00	9404	0.00	1204	0.17

4.4.1 CWE Distribution Map, PoR

First, the CWE frequencies per year were plotted and contoured for the PoR at an interval of one CWE per year from the data in Table 15. It was noted in Figure 11 that the top five CWE frequencies occurred at towers that were within three miles of the coast. Those towers (and locations) were 3131/3132 (central), 1101/1102 (coastal), 0061/0062 (coastal), 0020/0021 (coastal), and 0022 (coastal). Tower 3131/3132 is the most inland of these towers and was located on Merritt Island; it had a CWE frequency per year of 7.85. The other towers had frequency values of 7.56, 6.89, 6.40, and 5.92, respectively. The frequency range for the towers of lowest values fell below one, 0.17 to 0.72 CWE

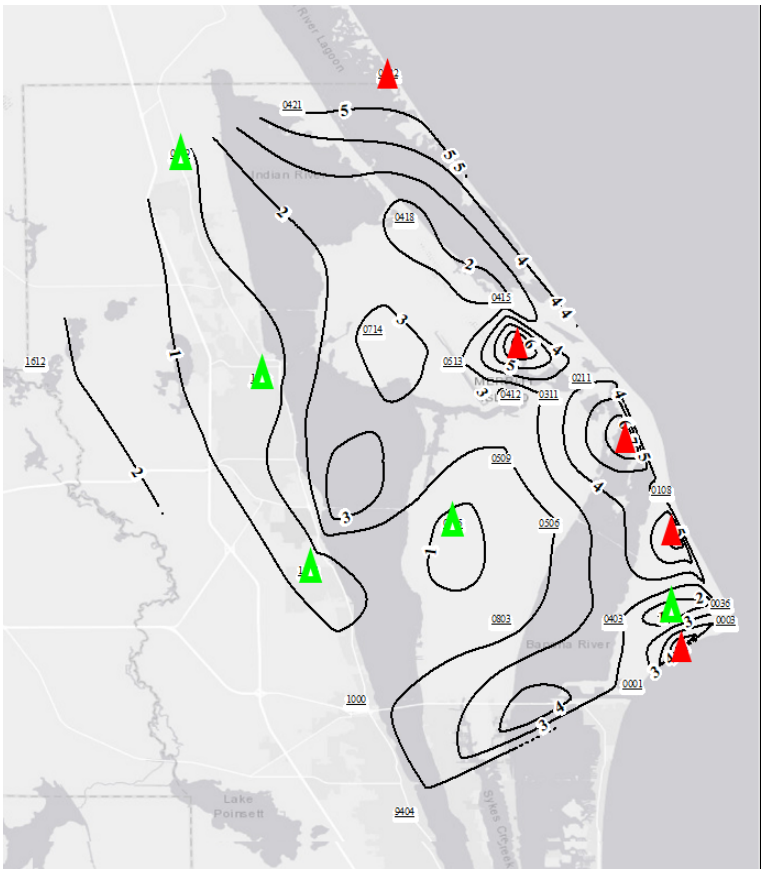

Figure 11. Geographic distribution of CWE frequency per year across the AoS with respect to the PoR. The red and green triangles represent the tower of highest and lowest CWE frequencies, respectively.

per year. The five lowest occurrences were at the towers of 0303 (coastal), 0819 (mainland), 0805 (central), 1012 (mainland), and 1204 (mainland). The last two towers listed here were consistently in the lowest two values for each WS month. The overall pattern for the PoR distribution of CWEs showed a coastal maxima and minima mostly at mainland towers.

4.4.2 CWE Distribution Map, WS months

The second category to be mapped was WS months. A smaller interval of 0.2 CWE per year was needed for mapping. This was because the frequency values for the months were smaller than those of the PoR (Table 9). These maps were further

categorized and analyzed as peak or transitional months. The geographic distribution of CWE frequency per year for peak months mimicked that of the PoR. The distribution of frequencies for June, July, and August indicated that the highest values were generally near the coast with a slight shift north or south depending on the month. The lowest values were commonly to the west and inland from the coast.

For the first peak month, June, the greatest values were concentrated over the southeastern part of the AoS (Fig. 12). The top five values ranged from 1.72 to 2.61 CWE per year. These values were recorded for the following towers as seen in Table 15: 1101/1102 (coastal), 3131/3132 (central), 0061/0062 (coastal), 0020/0021 (coastal), and 0300 (central). The last tower, 0300, was the furthest south and on the Banana River. The lowest values were mostly over the mainland with two scattered to the east over Merritt Island and Cape Canaveral like the lowest values for the PoR. Table 15 showed that the lowest values fell below 0.25 CWE per year. The five towers (and locations) of lowest values were: 0303 (coastal), 0805 (central), 0819 (mainland), 1204 (mainland), and 1012 (mainland). The map for June of geographic distribution of CWEs showed a general pattern for the highest and lowest frequencies that was similar to that for the PoR.

The second peak month, July, showed a similar pattern of CWE distribution as that of June but with a slight shift north of the maxima (Fig. 13); two of the highest frequencies occurred at the two most northern towers. July had four of the same high frequency towers as the PoR. The highest values ranged from 1.72 to 2.28 CWE per year and occurred at the following towers (and locations): 0022 (coastal), 3131/3132 (central), 0061/0062 (coastal), 0421 (central), 1101/1102 (coastal). The five towers of lowest

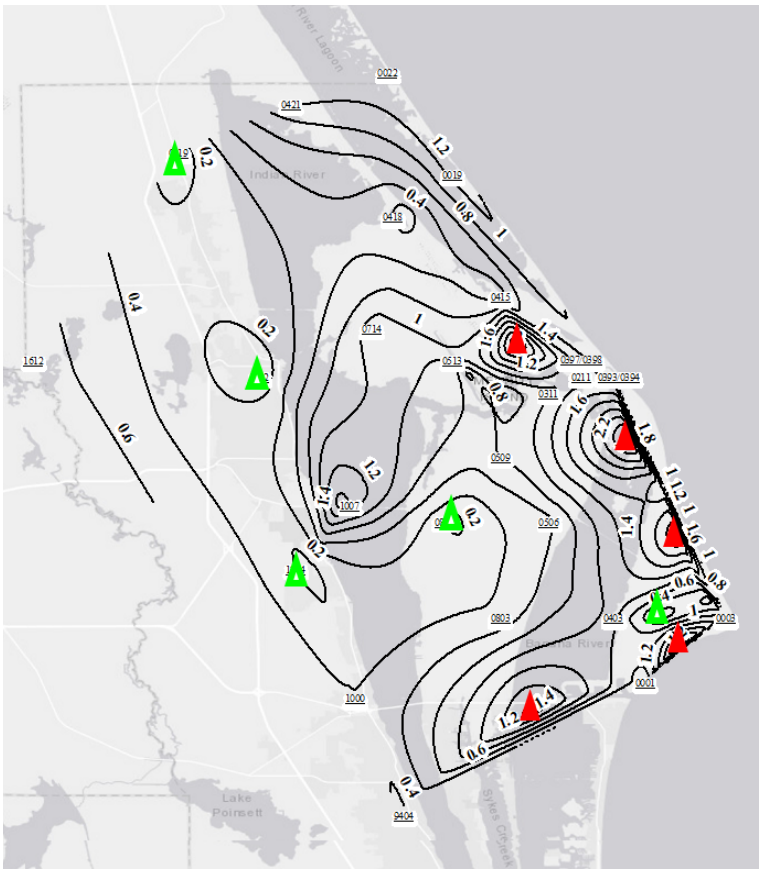

Figure 12. Geographic distribution of CWE frequency per year across the AoS with respect to June for the PoR. The red and green triangles represent the tower of highest and lowest CWE frequencies, respectively.

values all had frequencies of less than 0.30 CWE per year and occurred at the following towers (and locations): 9404 (mainland), 0303 (coastal), 0819 (mainland), 1012 (mainland), and 1204 (mainland). The map of geographic distribution of CWEs for July showed similar locations to those of the PoR for high and low frequencies.

The last month of peak convection to be mapped and analyzed was August. Again, the pattern was similar to that of the PoR, maxima were near the coast and minima were mostly inland as shown on the geographic distribution map (Fig. 14). The towers of top occurrences were noted as being the same towers as those of the PoR with a range

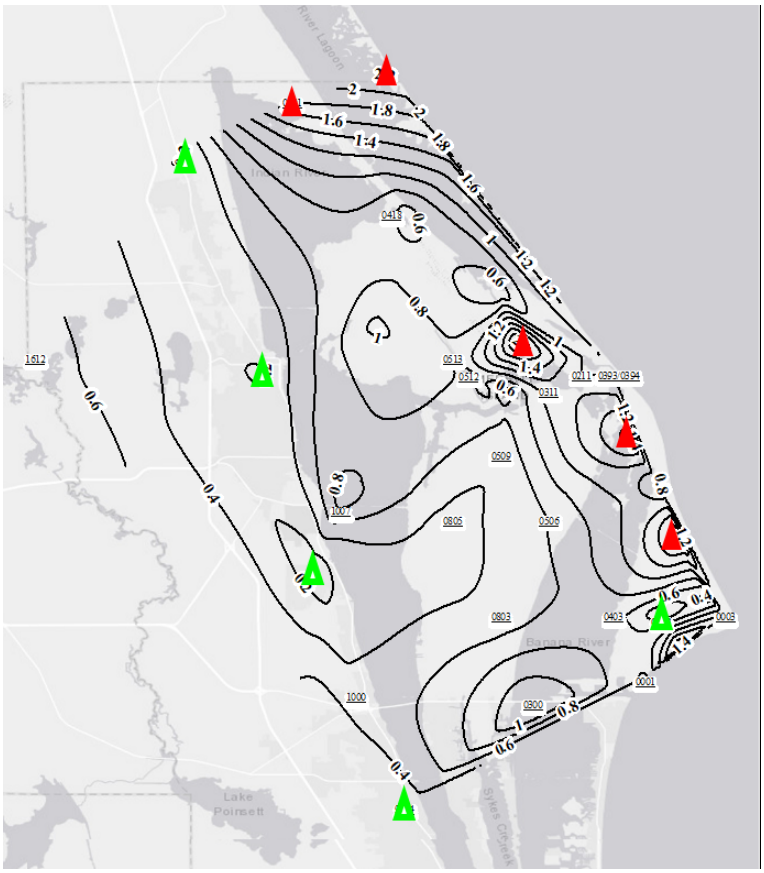

Figure 13. Geographic distribution of CWE frequency per year across the AoS with respect to July for the PoR. The red and green triangles represent the tower of highest and lowest CWE frequencies, respectively.

from 1.28 to 2.30 CWE per year. The towers of highest frequency for August were 3131/3132 (central), 0020/0021 (coastal), 1101/1102 (coastal), 0061/0062 (coastal), and 0022 (coastal). The pattern of frequency minima was more disperse compared to July and had a range of zero to 0.17 CWE per year. The towers of lowest frequencies were scattered from the mainland to Cape Canaveral; their TIDs (and locations) were 0803 (central), 0303 (coastal), 0805 (central), 1012 (mainland), and 1204 (mainland). The second subcategory of transition months had less associated convection and lower standard deviation which signified lower variation in the distribution of frequencies.

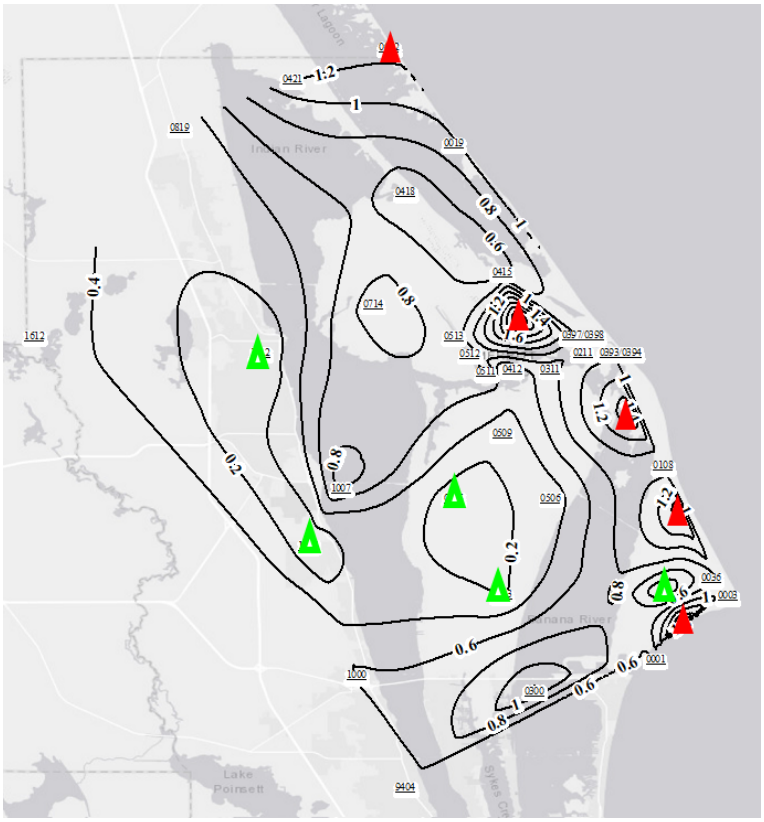

Figure 14. Geographic distribution of CWE frequency per year across the AoS with respect to August for the PoR. The red and green triangles represent the tower of highest and lowest CWE frequencies, respectively.

Still, the geographic distributions showed similar maxima locations as the PoR but the location and number of minima varied. Figure 15 showed the geographic distribution of CWE frequency across the area of study with respect to May. The top five towers of highest frequency for May had a range of 0.67 to 0.94 CWE per year (Table 15). The high frequencies were noted for the towers (and locations) of 1101/1102 (coastal), 0061/0062 (coastal), 3131/3132 (central), 0393/0394 (coastal), and 0421 (central). The low variation as discussed previously for the transition months made highlighting the minima on the maps complicated. The lowest five frequency values for May occurred at 12 towers. The purpose of mapping was to highlight the general areas of high and low

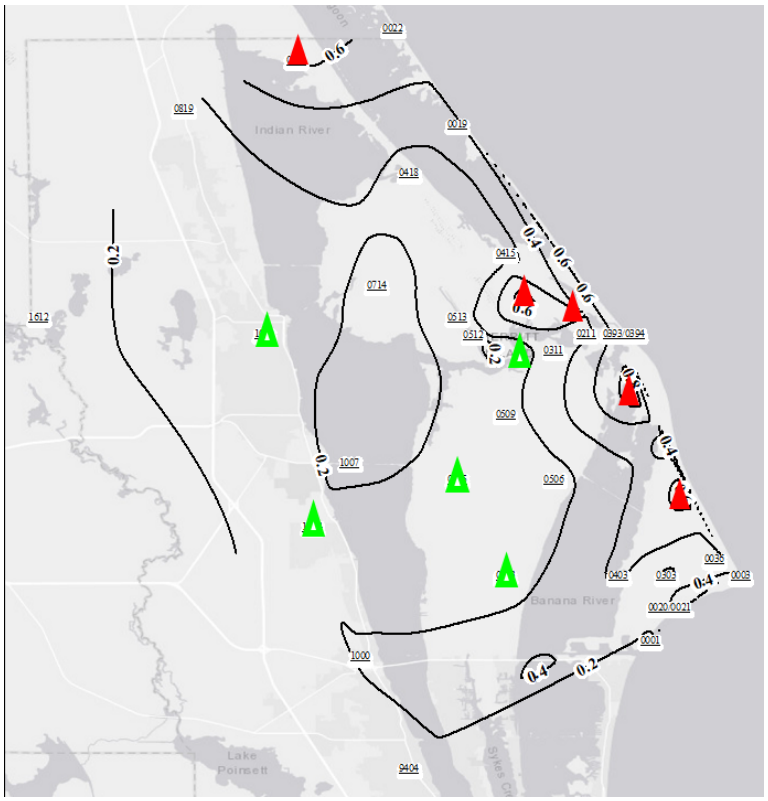

Figure 15. Geographic distribution of CWE frequency per year across the AoS with respect to May for the PoR. The red and green triangles represent the tower of highest and lowest CWE frequencies, respectively.

frequencies, thus it was unnecessary to highlight the 12 towers. Instead, the five towers of lowest values were marked on the map. These towers had a frequency range of zero to 0.08 CWE per year. The towers (and location) were 0805 (central), 0803 (central), 0412 (central), 1012 (mainland), and 1204 (mainland).

Next, the CWE distribution for September was mapped. The resultant pattern for this month mimicked the geographic frequency pattern of the PoR but with only four towers marked for the lowest values (Fig. 16). The five towers of highest frequency were 1101/1102 (coastal), 0061/0062 (coastal), 0020/0021 (coastal), 3131/3132 (central), and 0421 (central). The lowest frequency values for September occurred across 16 towers.

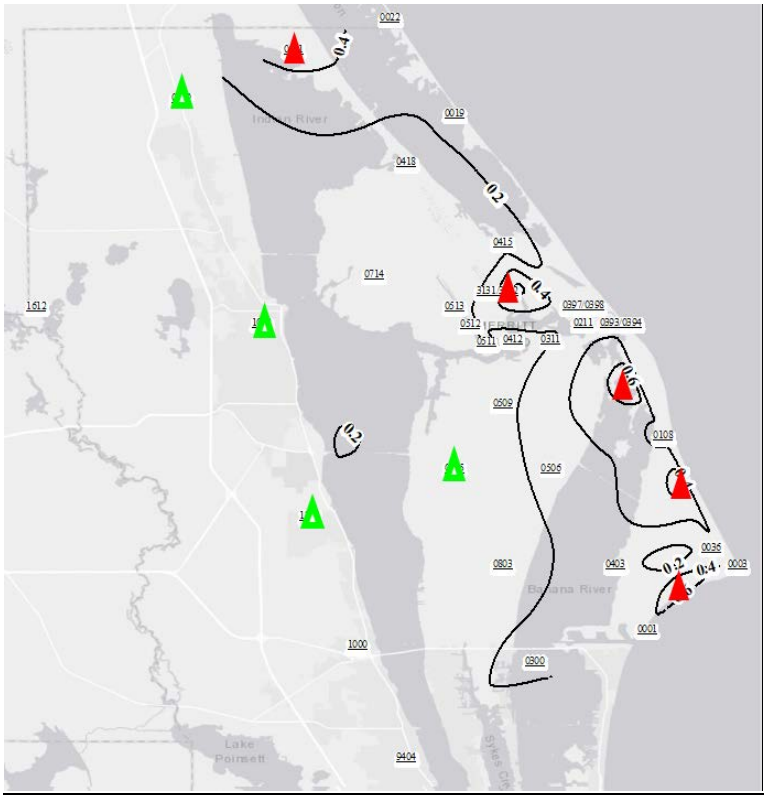

Figure 16. Geographic distribution of CWE frequency per year across the AoS with respect to September for the PoR. The red and green triangles represent the tower of highest and lowest CWE frequencies, respectively.

Four tower frequencies were equal to zero. The next lowest value was 0.06 and it occurred at seven towers. To avoid highlighting 16 towers only the four towers of zero CWE frequency were marked on the map. Those towers were 0805 (central), 0819 (mainland), 1012 (mainland), and 1204 (mainland). The matter of low standard deviation also occurred for some of the synoptic flow datasets.

4.4.3 CWE Distribution Map, Synoptic Flow Regimes

The CWE frequencies of the flow regimes were mapped based on the data in Table 16. This table was created from the data in Table 13 and formatted in the same way as Table 15. The co-located TIDs were accounted for in Table 16 as one location and the highest value of the two was retained in order to plot and contour the data. The

frequency cells of this table were color filled according to the geographic stratification shown in Figure 10. The cell colors for the mainland towers were gold; those in the central and Merritt Island area were left white; and the cells coastal areas were filled with light blue. The data for each regime was sorted in descending order of frequency. From Table 16 it was quickly noted that the highest frequencies for the regimes were mostly associated with coastal and central towers.

The pattern that emerged in the geographic distribution of CWEs for the PoR was nearly mimicked by those of the westerly flow regimes. The maps reflected the coastal maxima and mostly inland minima. It was noted from Table 16 that at least 60% of towers with the top five frequency values were in the coastal area. Under SW flows a majority (60%) of the five towers with the lowest values occurred at mainland locations; the other 40% occurred at varied locations across the AoS. This was illustrated in their associated maps as seen in Figures 17 and 18.

The SW-1 regime had the second highest convective activity based on the CP and CWE counts shown in Table 12. The frequency range for the top five towers of highest value was 1.67 to 2.67 CWE per year. The towers (and locations) were 1101/1102 (coastal), 3131/3132 (central), 0020/0021 (coastal), 0061/0062 (coastal), and 0022 (coastal); and were the same ones as those for the PoR. The five towers (and locations) of lowest values were 0819 (mainland), 0036 (coastal), 0805 (central), 1012 (mainland), 1204 (mainland). The map of geographic distribution of CWEs for the SW-1 regime showed a similar frequency pattern as that of the PoR.

The SW-2 regime was marked by the greatest convective activity of the six regimes. The towers of top five values for this regime were the same as those for SW-1

and the PoR. Those towers (and locations) were 3131/3132 (central), 1101/1102 (coastal), 0022 (coastal), 0061/0062 (coastal), 0020/0021 (coastal). The range of frequency for these towers was 2.28 to 3.56 CWE per year. The five towers of lowest frequencies were 0805 (central), 0303 (coastal), 0819 (mainland), 1204 (mainland), and 1012 (mainland). The contoured map with the marked towers of highest and lowest values showed the same locations of high and low frequencies as the PoR (Fig. 18).

The NW flow CWE frequencies created a pattern that was similar to that of the PoR but with slightly differed locations of the minima. The towers of top five values were over or near the coast. Their range of values was 0.72 to 0.89 CWE per year and

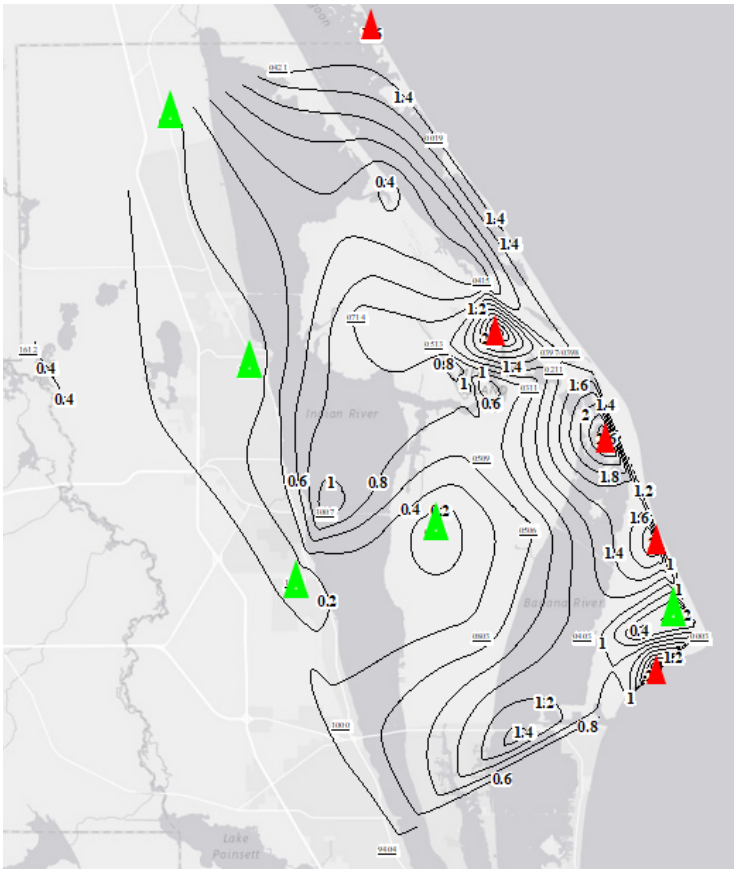

Figure 17. Geographic distribution of CWE frequency across the AoS with respect to the SW-1 flow regime for the PoR. The red and green triangles represent the tower of highest and lowest CWE frequencies, respectively.

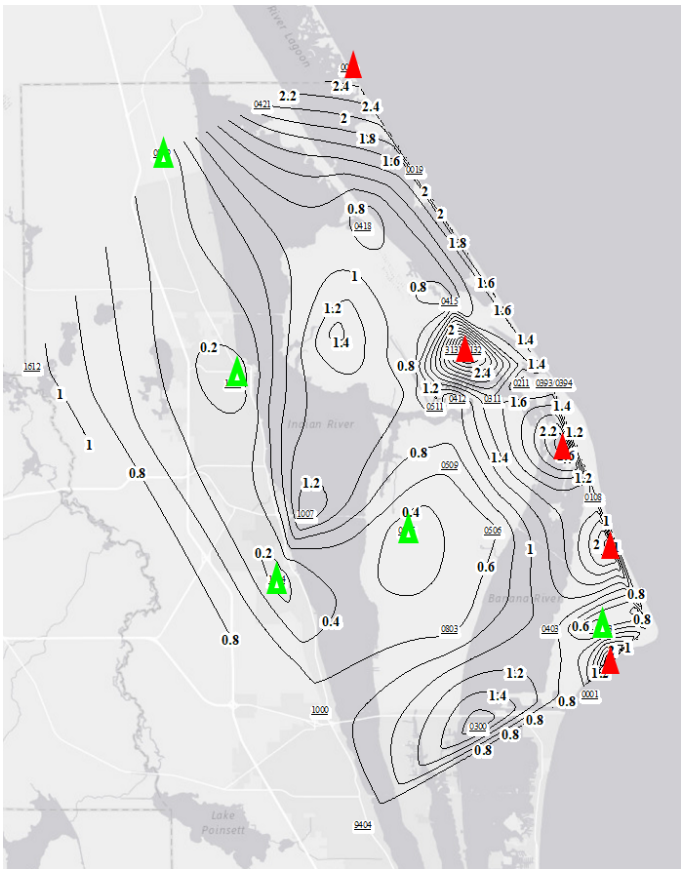

Figure 18. Geographic distribution of CWE frequency across the AoS with respect to the SW-2 regime for the PoR. The red and green triangles represent the tower of highest and lowest CWE frequencies, respectively.

occurred at the following towers: 1101/1102 (coastal), 0061/0062 (coastal), 0022 (coastal), 0300 (central), and 0421(central). The five towers of lowest frequencies were spread across the AoS and had values ranged from 0.06 to 0.17 CWE per year. The towers (and locations) were 0001 (coastal), 0303 (coastal), 1012 (mainland), 1204 (mainland), and 0803 (central). The geographic distribution of CWE for the NW regime showed a general pattern of coastal maxima and minima that were scattered across the AoS (Fig. 19).

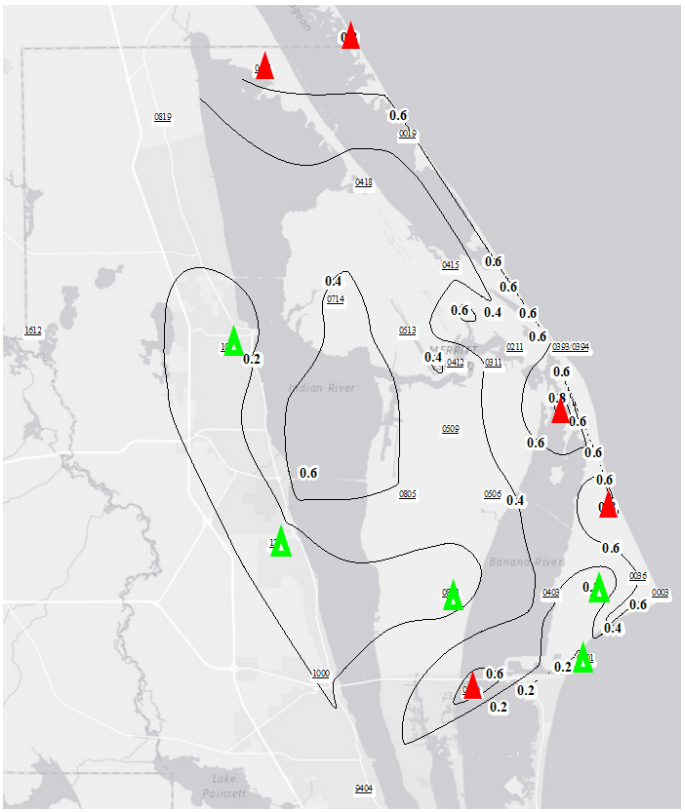

Figure 19. Geographic distribution of CWE frequency across the AoS with respect to the NW regime for the PoR. The red and green triangles represent the tower of highest and lowest CWE frequencies, respectively.

The CWE frequencies for each easterly flow had smaller spreads and lower variations so it was complicated to describe the high and low frequencies because the values were not unique to five towers. The overall pattern for the easterly regimes reflected the near coastal maxima but the pattern exhibited by the minima were dissimilar to locations shown for the PoR. The variation in spread for easterly regimes was low compared to the westerly regimes. Lower variation indicates more uniform distribution of frequency values across the AoS. Consequently, there were some instances where it was not possible to mark five towers for lowest and highest values.

The first easterly flow, SE-1 had maxima similar to those of the PoR but the minima were located at mostly central locations. The range of values for the top six towers was 0.39 to 0.53 CWE per year. Six towers were marked on the map (Fig. 20) because these towers were associated with the top five values. This was a consequence of lower variation in frequency values. The towers (and locations) were: 0020/0021 (coastal), 0421(central), 3131/3132 (central), 0022 (coastal), 0061/0062 (coastal), and 1101/1102 (coastal). The lowest five values of SE-1 (and their recurrence) were 0.00 (4), 0.06 (9), 0.11 (6), 0.12 (2), and 0.20 (1); these values were distributed among 22 towers across the AoS. Only the four towers with frequency values of zero were marked on the map to keep with highlighting a general area of low frequencies. Those towers (and locations) were 0415 (central), 0418 (central), 0805 (central), and 0819 (mainland). The contoured map with the marked towers of highest and lowest values showed the same general locations of coast maxima but the minima occurred mostly over Merritt Island (Fig. 20).

The second easterly flow mapped was SE-2. The five towers of highest frequency were typically located over the coastal region. The range of these values was 0.18 to 0.29 CWE per year. The towers (and locations) were 0003 (coastal), 0020/0021 (coastal), 1007 (central), 0036 (coastal), and 0019 (coastal). The lowest five values for SE-2 were 0.00, 0.06. 0.07, 0.11, and 0.12; these values occurred at 28 tower locations across the AoS. The lowest frequency was zero and occurred at 13 towers across the AoS as listed here: 0022 (coastal), 0108 (coastal), 0303 (coastal), 0412 (central), 0415 (central), 0506 (central), 0509 (central), 0803 (central), 0805 (central), 0819 (mainland), 1000 (mainland), 1012 (mainland), and 1204 (mainland). The geographic distribution of

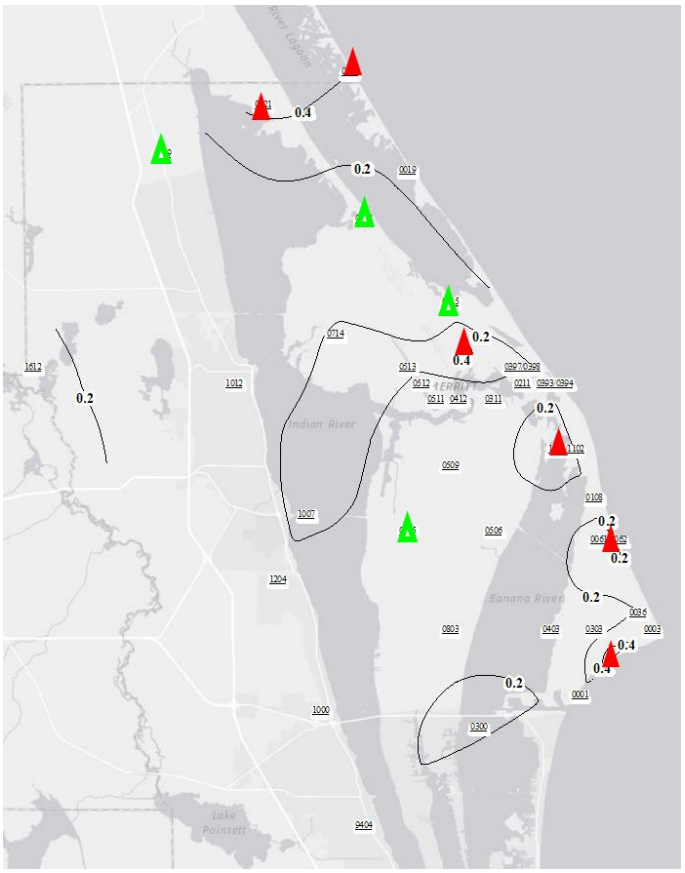

Figure 20. Geographic distribution of CWE frequency across the AoS with respect to the SE-1 regime for the PoR. The red and green triangles represent the tower of highest and lowest CWE frequencies, respectively.

CWEs for the SE-2 regime showed mostly coastal maxima and minima that were scattered across the AoS (Fig. 21).

The NE flow regime had the lowest standard deviation about the mean which signifies that it also had the lowest variation in values. The towers (and locations) that had the top five values of CWE frequency per year were 0061/0062 (coastal), 1101/1102 (coastal), 0020/0021 (coastal), 0393/0394 (coastal), and 0211 (coastal). The frequency range of these towers was 0.11 to 0.28 CWE per year. There were 21 towers across the AoS with a frequency of zero CWE per year. These towers (and locations) were 0001

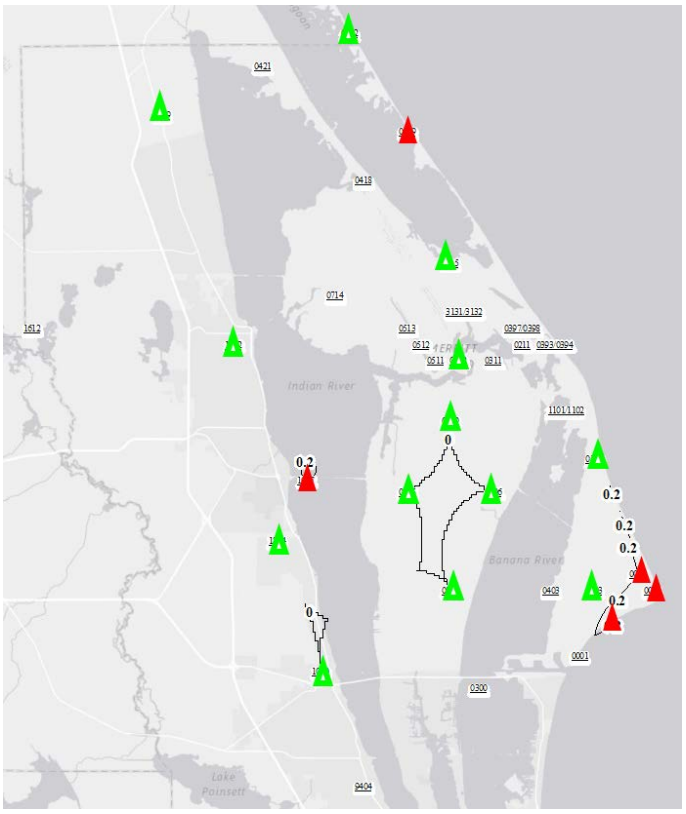

Figure 21. Geographic distribution of CWE frequency across the AoS with respect to the SE-2 regime for the PoR. The red and green triangles represent the tower of highest and lowest CWE frequencies, respectively.

(coastal), 0019 (coastal), 0108 (coastal), 0300 (central), 0415 (central), 0418 (central), 0421(central), 0506 (central), 0509 (central), 0511 (central), 0512 (central), 0513 (central), 0714 (central), 0803 (central), 0805 (central), 0819 (mainland), 1000 (mainland), 1012 (mainland), 1204 (mainland), 1612 (mainland), and 9404 (mainland). The contoured map with marked towers of highest and lowest values again showed coastal maxima but the minima were dispersed across the AoS (Fig. 22).

This chapter presented the CWE frequencies with respect to the PoR, WS months, and flow regimes. After mapping the various regimes two feature stood out: 1.) there were zero red markers of highest occurrence over the mainland and 2.) SW-1 and SW-2

most closely mimic the geographic distribution of CWE frequencies for the PoR. The next chapter will discuss the thought behind the emerged patterns and future work.

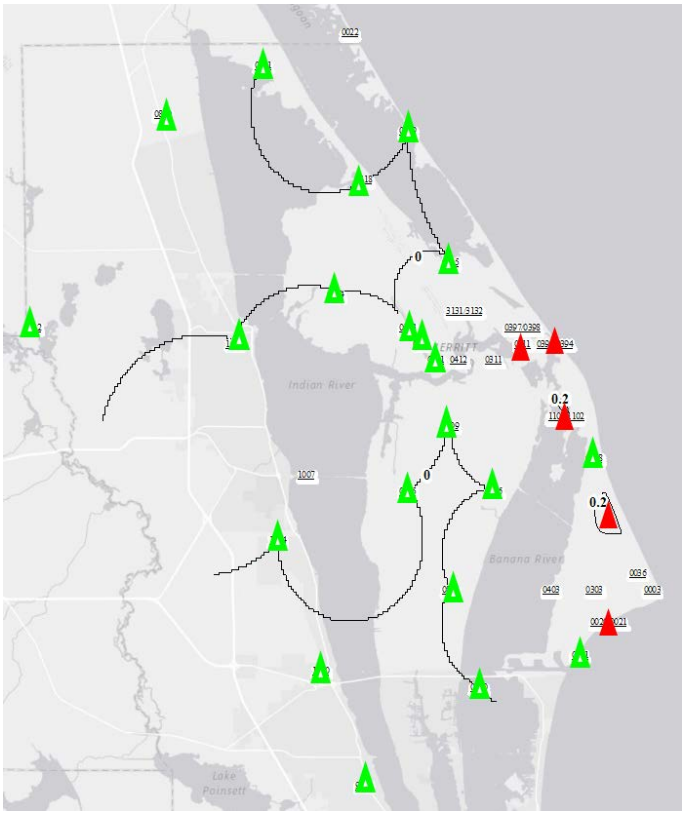

Figure 22. Geographic distribution of CWE frequency across the AoS with respect to the NE regime for the PoR. The contouring has many unreal features due to the very low number of events under this flow regime. The red and green triangles represent the tower of highest and lowest CWE frequencies, respectively.

V. Conclusions and Recommendations

The purpose of this research was to support impact planning; to determine how often a specific grid point within the surrounding area of CCAFS/KSC experienced downburst winds GTE 35 kt on average per year. In order to do this, the occurrence of CWEs across the AoS were determined and mapped to provide a geographic distribution of CWE frequency per year with respect to the PoR, WS months, and synoptic flow. The contoured maps of CWE rate were generated to assist with interpolation of occurrence at non-tower locations. The CWE rate was calculated using 5-minute peak wind observations from the Cape/WINDS mesonet of 42 towers between May to September of 1995-2012. In this chapter the results of the analysis were discussed, topics of future study were suggested, and the study summarized.

5.1 PoR and WS Months

A distinct geographic pattern in the frequency distribution was apparent for the PoR. This was of a coastal maxima and minima that occurred mostly inland. The patterns generated from the WS month datasets were similar to that of the PoR despite the seasonal differences among the frequency spreads. And so, it was noted that although convective activity changed seasonally the general pattern of where the highest and lowest frequencies occurred did not. While an eastward displacement was expected for downburst frequency from the mainland lightning frequency (Figure 23; W. P. Roeder, personal communication, July 1, 2017), the displacement was much stronger than expected, showing a very strong preference along the coast of CCAFS/KSC. Figure 23 showed the mean cloud-to-ground lightning flash density for the AoS and was compiled

from the National Lightning Detection Network for the years of 1997-2013. This figure showed maxima of approximately 13-21 flashes per km^2 concentrated over the mainland decreasing values with approach to the coast.

5.2 Synoptic Regime

Analysis of CWE frequency as a function of regime revealed dissimilarities among the frequency spreads of westerly versus easterly flow regimes. Statistically significant differences were found between the two subcategories through application of the bootstrap method to determine the standard deviation of frequency distribution for each regime dataset (Fig. 9). It was determined with 90% confidence that the frequency

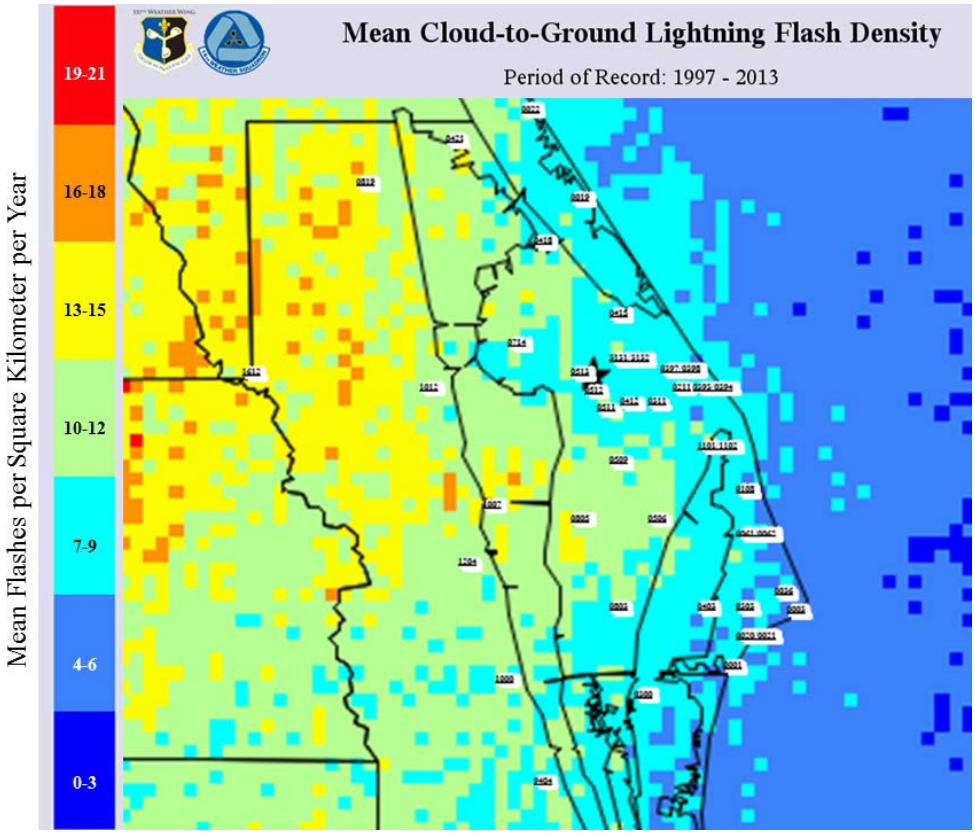

Figure 23. The annual mean cloud to ground lightning flash density for the AoS compiled for 1997-2013 (W. P. Roeder, personal communication, July 1, 2017).

distributions of westerly and easterly components were different. The standard deviation for westerly regimes was higher than that of easterly regimes. This suggests the frequency distribution of westerly flows had greater variation which resulted in concentrated areas of high and low CWE rates. Conversely, easterly regimes had lower standard deviations that resulted in a less varied frequency distribution that resulted in a geographic distribution of CWE frequency of a coastal maxima but minima that were greater in number and dispersed across the AoS.

The dominating pattern of coastal maxima and inland minima was likely the result of complex interactions between prevailing and local winds. Gentry and Moore (1954) explained that prevailing winds impact local wind circulations and thus the spatial and temporal variation in convective activity across the Florida Peninsula. During Florida's WS the westerly flow regimes occurred more often than the easterly regimes. The total percentage of flow regime days (Table 17) was determined and showed that prevailing westerly flow occurred with regularity at about 48% of all days within the warm season. This was followed by easterly regimes at nearly 40% of days and then by the "Other" at nearly 13% (Lambert 2007).

Southwest flow dominated Florida's WS (Lericos 2002; Lambert 2007) and so the composite distribution and geographic pattern was most influenced by this prevailing wind. SW-2 occurred with most regularity for the PoR (Table 17; Lambert 2007). SW1/2 occurred at approximately 36% of the total WS days. This was important to note because the interaction of prevailing wind with local wind influenced the spatial and temporal distribution of convection across Florida (Gentry and Moore 1954; Lericos et al. 2002). Two major diurnal sea-breeze circulations occurred with regularity over Florida

Table 17. Total percentage of flow regime days (Lambert 2007).

	SW-1	SW-2	NW	SE-1	SE-2	NE	Other
PoR	11.8%	23.8%	12.1%	17.2%	9.8%	12.5%	12.8%

during the period of analysis; they are the 1.) west coast (Gulf of Mexico) sea breeze and 2.) the east coast (Atlantic Ocean) sea breeze. Modifications of the east coast sea breeze by the prevailing wind were of importance for explaining the prominent geographic pattern that prevailed for the PoR and the WS months.

The resultant pattern of geographic distribution frequency for SW-1 and SW-2 (SW1/2) nearly replicated that of the PoR. The five towers of highest CWE frequencies for SW1/2 were the same as for the PoR. Additionally, 80% of the five towers with the lowest frequencies for both SW1/2 were shared with the PoR. Because SW1/2 occurred so regularly they were the regimes of most influence for the PoR.

Gentry and Moore (1954) postulated that strong afternoon convection more frequently occurred near downwind coasts where the prevailing flow would oppose and retard the development of the sea-breeze circulation. This delay resulted in strong afternoon convection. The AoS was in a location where its local sea-breeze would be opposed by the SW1/2 regimes which resulted in a convection, development and decay, occurring most often in the afternoon and near the coast. Additionally, the occurrence of convection is enhanced by the greater availability and uptake of energy from heating as the air mass traverses the peninsula from the southwest towards the Atlantic coast. Greater and stronger convection result in higher thunderstorms which subsequently result in stronger downdrafts due to the increased time for acceleration from higher heights

compared to weaker thunderstorms of lesser height. This was a possible explanation for why the towers of highest observed CWE frequencies were near the coast.

Dinon et al. (2008) postulated that the sea-breeze front (SBF) was an important feature in convective cell initiation. It was found that a majority (54%) of cells that produced winds GTE 35 kt were initiated in one of two ways: 1) by a sea-breeze front alone (SBF) or 2) the merger of a sea-breeze front and an outflow boundary (SBF and OFB). Approximately 16% of these cells were initiated by the SBF and 38% by SBF and OFB. The secondary convection initiated by the SBF and OFB was an additional and important factor in the occurrence of CWE near the coast.

5.3 Future work

The downburst frequency for the entire AoS was previously known, but the geographical distribution across the AoS was not. The results of this research determined a distinctive non-uniform pattern. A future project might include the investigation of maximum wind speed distribution at each tower location so that the probability of meeting or exceeding any speed threshold, given that convective winds occur, can be found.

Yet another possible future project is normalizing the downburst frequency to the same 300 ft tower reporting level. Most of the towers have a highest reporting height of 54 ft, but others have higher heights. Since the 45 WS convective wind warnings are for up to 300 ft, the analysis would benefit for using the surface to the highest height which should include the highest wind speeds due to reduced surface friction. In particular, this may reduce the magnitude of the local maxima of downburst frequency in this analysis at

the highest towers and reveal a more representative pattern of downburst frequency across CCAFS/KSC. But, preliminary work still suggests that there is still a preference for the maxima near the coast and the contour map in Figure 24 illustrates this. The map is for the PoR with some data omitted; that data is for the towers with sensors at greater than 54 ft AGL.

Finally, the downburst analysis should be expanded to include the warm seasons at CCAFS/KSC since the last year the Plymouth State University database. This will increase the sample size and yield more statistically robust results.

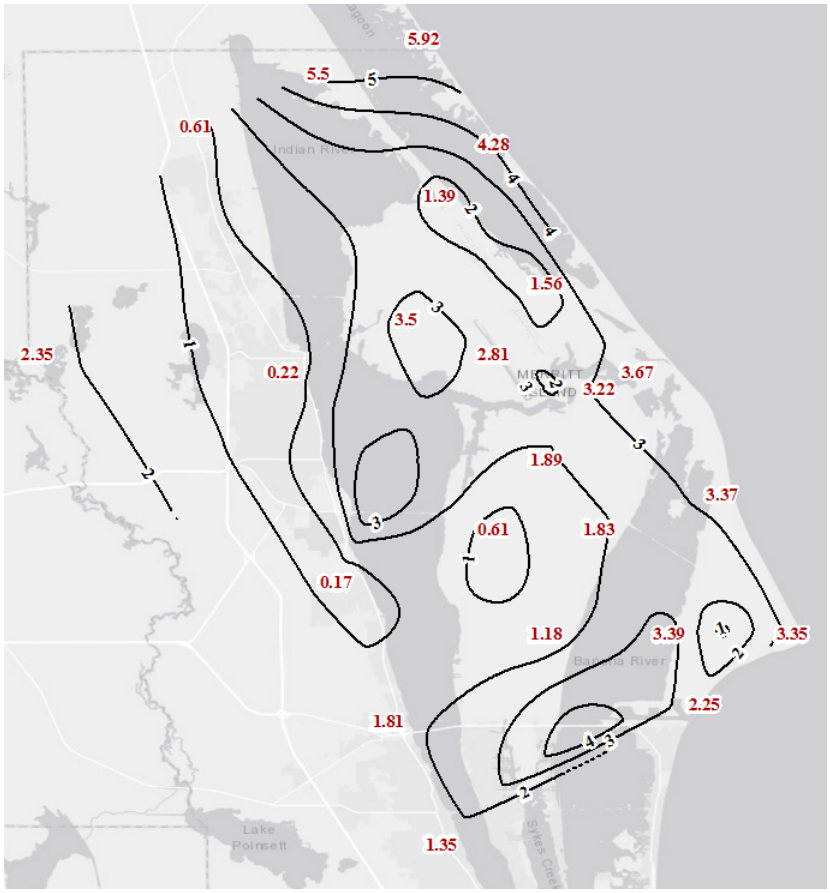

Figure 24. Geographic distribution of CWE frequency per year as in Figure 11, except with the data for towers with sensors at greater than 54 ft AGL removed. The frequencies are in red and the contours are for 1 CWE per year.

Bibliography

14th WS, 2016: Operational Climatic Data Summary (OCDS-II), 2.6.1.2. 14th Weather Squadron, accessed 1 September 2017, https://www.afccc.af.mil.

Ander C. J., A. J. Frumkin, J. P. Koermer and W. P. Roeder, 2009: Study of sea-breeze interactions which can produce strong warm-season convective winds in the Cape Canaveral area. *16th Conf. on Air-Sea Interaction/8th Conf. on Coastal Atmospheric and Oceanic Prediction and Processes*, January, Phoenix, AZ.

Atkins, N.T. and R.M. Wakimoto, 1991: Wet Microburst Activity over the Southeastern United States: Implications for Forecasting. *Wea. Forecasting*, **6**, 470–482, doi: 10.1175/1520-0434(1991)006<0470:WMAOTS>2.0.CO;2.

Cummings, K. A., E. J. Dupont, A. N. Loconto, J. P. Koermer and W. P. Roeder, 2007. An updated warm-season convective wind climatology for the Florida Space Coast. Preprint CD-ROM, *16th Conf. of Applied Climatology*, January, San Antonio, TX.

Dinon, H. A., M. J. Morin, J. P. Koermer, and W. P. Roeder, 2008. Convective winds at the Florida Spaceport: year-3 of Plymouth State research. *13th Conf. on Aviation, Range, and Aerospace Meteorology*, January, New Orleans, LA.

Eastern Range Instrumentation Handbook, 2017: WINDS, Eastern Range Instrumentation Handbook, Patrick AFB, FL 32925, 14 Apr 2017, 27 pp.

Fujita, T. T. 1985: The downburst: Microburst and macroburst. SMRP Research Paper 210, University of Chicago, 122 pp. [NTIS PB85-148880.]

Gentry, R.C. and P.L. Moore, 1954: Relation of Local and General Wind Interaction Near the Sea Coast to Time and Location of Air-Mass Showers. *J. Meteor.*, **11**, 507–511, https://doi.org/10.1175/1520-0469(1954)011<0507:ROLAGW>2.0.CO;2

Harms, D. E., A. A. Guiffrida, B. F. Boyd, L. H. Gross, G. D. Strohm, R. M. Lucci, J. W. Weems, E. D. Priselac, K. Lammers, H. C. Herring and F. J. Merceret, 1999: The many lives of a meteorologist in support of space launch, Preprints, *8th Conf. On Aviation, Range, and Aerospace Meteorology*, Dallas, TX, 5-9.

Koermer, J. P., and W. P. Roeder, 2008. Assessment of the importance of certain wind towers in the Cape Canaveral AFS/Kennedy Space Center mesonet for predicting convective winds. 13th Conf. on Aviation, Range, and Aerospace Meteorology, January, New Orleans, LA.

Koermer, J.P., 2017: Plymouth State University Meteorology CCAFS/KSC Warm-Season Convective Wind Climatology. 1 October 2017, https://vortex.plymouth.edu/conv_winds/.

Lambert, W. C., 2002. Statistical short-range guidance for peak wind speed forecasts on Kennedy Space Center/Cape Canaveral Air Force Station: Phase I results. NASA Contractor Report CR-2002-211180. 39 pp.

Lambert, W. C., 2007. Objective Lightning Probability Forecasting for Kennedy Space Center and Cape Canaveral Air Force Station, Phase II. NASA Contractor Report CR-2007-214732. 59 pp.

Lericos, T. P., H. E. Fuelburg, A. I. Watson, and R. I. Holle, 2002: Warm season lightning distributions over the Florida Peninsula as related to synoptic patterns. *Weather and Forecasting*, **17**, 83-98.

Loconto, A. N., J. P. Koermer, and W. P. Roeder, 2006. An updated warm-season convective wind climatology for Cape Canaveral Air Force Station/Kennedy Space Center. *12th Conf. on Aviation, Range, and Aerospace Meteorology*, Atlanta GA.

Lupo, Kevin M., 2013. An update to the convective wind climatology of Kennedy Space Center/Cape Canaveral Air Force Station, *12th Annual Student Conference*, Amer. Meteor. Soc., Austin, TX.

McCue, M. H., J. P. Koermer, T. R. Boucher, and W. P. Roeder, 2010. Validations and development of existing and new RAOB-based warm-season convective wind forecasting tools for Cape Canaveral Air Force Station and Kennedy Space Center, *22nd Conference on Climate Variability and Change*, Atlanta, GA,.

Orloff, J., J. Bloom, 2014: Bootstrap confidence intervals. MIT OpenCourseWare, Accessed 1 December 2017, https://ocw.mit.edu/courses/mathematics/18-05-introduction-to-probability-and-statistics-spring-2014/readings/MIT18_05S14_Reading24.pdf.

Penn State/Department of Statistics Online Programs, 2017: STAT 415 Intro Mathematical Statistics. Eberly College of Science, 29 December 2017, https://onlinecourses.science.psu.edu/stat414/node/289.

Rauber, R. M., J. E. Walsh, D. J. Charlevoix, 2008: *Severe and hazardous weather, an introduction to high impact meteorology 3rd edition*, Kendall/Hunt Publishing, 642 pp.

Roeder, W. P., L. L. Huddleston, W. H. Bauman III, and K. B. Doser, 2014. Weather research requirements to improve space launch from Cape Canaveral Air Force Station and NASA Kennedy Space Center, *1st Annual Conference in Space Traffic Management Conference.* Paper 14.

Sanger, N. T., 1999: A four-year summertime microburst climatology and relationship between microbursts and cloud-to-ground lightning flash rate for the NASA Kennedy Space Center, Florida: 1995-1998, M.S. Thesis, Texas A&M University, 116 pp.

Wilson, J. W. and R. M. Wakimoto, 2001: The discovery of the downburst: T. T. Fujita's contribution. *Bull. Amer. Meteor. Soc*., **82**, 49–62, doi: 10.1175/1520-0477(2001)082<0049:TDOTDT>2.3.CO;2.

REPORT DOCUMENTATION PAGE

Form Approved
OMB No. 074-0188

1. REPORT DATE *(DD-MM-YYYY)*	**2. REPORT TYPE**	**3. DATES COVERED** *(From – To)*
22-03-2018	Master's Thesis	October 2016 – March 2018

TITLE AND SUBTITLE

The geographic distribution of downburst frequency across Spaceport Florida

5a. CONTRACT NUMBER

5b. GRANT NUMBER

5c. PROGRAM ELEMENT NUMBER

6. AUTHOR(S)

Garza, Tania M., Captain, USAF

5d. PROJECT NUMBER

5e. TASK NUMBER

5f. WORK UNIT NUMBER

7. PERFORMING ORGANIZATION NAMES(S) AND ADDRESS(S)

Air Force Institute of Technology
Graduate School of Engineering and Management (AFIT/EN)
2950 Hobson Way, Building 640
WPAFB OH 45433-8865

8. PERFORMING ORGANIZATION REPORT NUMBER

AFIT-ENP-MS-18-M-082

9. SPONSORING/MONITORING AGENCY NAME(S) AND ADDRESS(ES)

45th Weather Squadron
1201 Edward H. White II St., MS 7302
Patrick AFB, FL 32925-3238
321-853-8410 and william.roeder@us.af.mil
ATTN: William P. Roeder

10. SPONSOR/MONITOR'S ACRONYM(S)

45 WS

11. SPONSOR/MONITOR'S REPORT NUMBER(S)

12. DISTRIBUTION/AVAILABILITY STATEMENT

DISTRIBUTION STATEMENT A. APPROVED FOR PUBLIC RELEASE; DISTRIBUTION UNLIMITED.

13. SUPPLEMENTARY NOTES

14. ABSTRACT

Strong winds from downbursts pose a significant hazard to personnel and launch operations at Cape Canaveral Air Force Station (CCAFS) and NASA Kennedy Space Center (KSC). The CCAFS/KSC complex has a robust mesonet from which an 18 year (1995-2012) warm-season convective wind climatology (WSCWC) was developed (Koermer 2017). While the frequency of downbursts in the area has been determined, the frequency at the individual tower locations has not. The 5-minute peak wind data from the WSCWC was analyzed to determine the geographic distribution of downburst frequency across Spaceport Florida. For this project a downburst was determined by the threshold of peak wind speeds greater than or equal to 35 kt. Data for each individual tower in the mesonet was analyzed to determine the frequency of downburst at that grid point. A distinct pattern emerged that showed downburst maxima near the coast and minima mostly over the mainland. It was hypothesized that Florida flow regimes have a significant influence on thunderstorm initiation and subsequent downbursts (Dinon et al. 2008, McCue et al. 2010, Lupo 2013).

15. SUBJECT TERMS

Convective Winds, Cape Canaveral, Downbursts, Downburst Frequency

16. SECURITY CLASSIFICATION OF:			**17. LIMITATION OF ABSTRACT**	**18. NUMBER OF PAGES**	**19a. NAME OF RESPONSIBLE PERSON**
a. REPORT	**b. ABSTRACT**	**c. THIS PAGE**			Omar A. Nava, AFIT/ENP
U	**U**	**U**	**UU**	68	**19b. TELEPHONE NUMBER** *(Include area code)* (937) 255-3636, ext 4519(NOT DSN) (Omar.Nava@afit.edu)

Standard Form 298 (Rev. 8-98)
Prescribed by ANSI Std. Z39-18